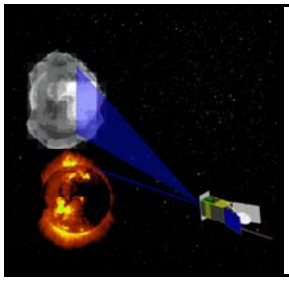

Istituto di Fisica dello Spazio Interplanetario

Scientific and Technical Plan

SCENARIO
NSWD
(Neutral Solar Wind Detector)

ESA / NASA - Solar Orbiter

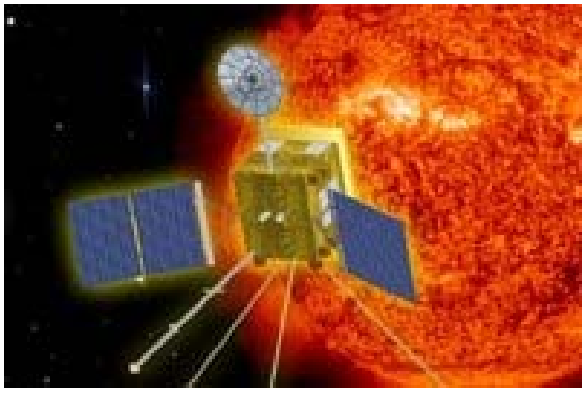

prepared by	SCENARIO NSWD TEAM		
approved by	Stefano Orsini, Principal Investigator (INAF-IFSI)		
endorsed by	Enrico Flamini (Agenzia Spaziale Italiana)		
reference	SO-NSW-PL001		
Issue	1	revision	0
date of issue	JANUARY 2008		

DISTRIBUTION

name	organization
Solar Orbiter Project Office	ESA and related Solar Orbiter Program Science Panel & Industrial working team.

CHANGE LOG

date	issue	revision	pages	reason for change
January 2008	1	0		1st Issue

ACRONYM LIST

ADC Analog to Digital Converter

AIT Assembly Integration and Test

AI&V Assembly Integration and Verification

AMU Atomic Mass Unit

APE Analog Proximity Electronics

APID APplication IDentifier

ASIC Application Specific Integrated Circuit

BOL Beginning Of Life

CBE Current Best Estimation

CCEM Ceramic Channel Electron Multiplier

CDMU Command Data Management Unit

CEM Channeltron Electron Multiplier

CM Common Mode

CME Coronal mass Ejection

CoG Centre of Gravity

CoM Centre of Mass

CR Collection Rate

DAC Digital to Analog Converter

DC Direct Current

DHSU Data Handling Support Unit

DM Differential Mode

DMA Direct Memory Access

DOF Degrees Of Freedom

DPU Data Processing Unit

DS Document Specification

DSP Digital Signal Processor

EBL Electron Beam Lithography

EGSE Electric Ground Support Equipment

ELENA Emitted Low Energy Neutral Atom

EM Electro Magnetic

EM Engineering Model

EMI Electro Magnetic Interferences

EMC Electro Magnetic Compatibility

EM/STM Engineering Model/Structural Model

ENA Energetic Neutral Atoms

EOL End Of Life

ESA Electrostatic Analyser

FEE Front End Electronics

FIFO First In-First Out

FM Flight Model

FOV Field Of View

FPGA Field Programmable Gate Array

FS Flight Spare

GF Geometrical Factor

HBR High Bit Rate

H-ENA High Energy Neutral Atoms

HK HouseKeeping

HPU Hub Processor Unit

HRC High Resolution Camera

HV High Voltage

HVPS High Voltage Power Supply

IBDR Instrument Baseline Design Review

ICD Interface Control Document

ICDR Instrument Critical Design Review

I/F InterFace

IFAR Instrument Flight Acceptance Review

IFE Instrument Front End

IFOV Intrinsic Field Of View

IHDR Instrument Hardware Design Review

IPDR Instrument Preliminary Design Review

IQR Instrument Qualification Review

ISM Interstellar Medium

ISRR Instrument Science Requirements Review

ISVR Instrument Science Verification Review

LAN Local Area Network

L-CAM Limb Camera

LCL Latching Current Limiter

LSB Least Significant Bit

LUT Look Up Table

MBR Medium Bit Rate

MCP Micro Channel Plate

MENA Medium Energy Neutral Atoms

MGSE Mechanical Ground Support Equipment

MICD Mechanical Interface Control Document

MLI Multi Layer Insulation

MOC Mission Operation Centre

MoI Moment of Inertia

MSB Most Significant Bit

NSW Neutral Solar Wind

NSWD Neutral Solar Wind Detector

OBDH On Board Data Handling

PA Product Assurance

PAEX Pluto Atmosphere Escape Experiment

PCB Power Control Box

PCB Printed Circuit Board

PDR Preliminary Design Review

PDD Payload Definition Document

PDU Power Distribution Unit

PEEK PolyEthereEtherKetone

PG Pulse Generator

PHA Pulse Height Analysis

PMI Piccola Media Impresa –(Italian Small/Medium size enterprise category)

PRS Pseudo Random gate Sequence

PSD Power Spectrum Density

PTI Product Tree Item

QA Quality Assurance

QM Qualification Model

RIE Reactive Ion Etching

RPA Retarding Potential Analyser

RTOS Real Time Operating System

RTU Remote Terminal Unit

S/C SpaceCratft

SCENARIO Solar Corona ENA Radiation Imagine Observer

SCU System Control Unit

SEL Single Event Latch-up

SEP Solar energetic Particle

SERENA Search for Exospheric Refilling and Emitted Natural Abundances

SIS Spacecraft Interface Simulator

SMD Surface Mounted Devices

SMM Structural Mathematical Model

SolO Solar Orbiter

SOC Science Operation Centre

STM Structural Thermal Model

SYS System

SW Solar Wind

SWA Solar Wind Analyser

SWT Solar system Working group

TBC To Be Confirmed

TBD To Be Defined

TBW To Be Written

TC TeleCommand

TDC Time to Digital Converter

TM Telemetry

TMM Thermal Mathematical Model

TOF Time Of Flight

TRP Temperature Reference Point

TRR Test Readiness Review

TV Thermal Vacuum

UORF Unit Optical Reference Frame

UPA Ultrasonic Piezo Actuator

URF Unit Reference Frame

UVCS Ultra Violet Coronograph Spectrometer

UVS Ultra Violet Spectrometer

APPLICABLE DOCUMENTS

AD1: SOL-EST-IF-0050 “SOLO EID-A”, Version 1 Rev 0, 9 October 2007

SOL-EST-SP-00705, “Solar Orbiter Payload Definition Document”, 3 October 2007

SCI-S/2007/157, “Solar Orbiter Science Management Plan“, 15 October 2007

SCI-SH/2005/100/RGM, “Solar Orbiter Science Requirements Document“, 31 March 2005

COVER PAGE

PI, TEAM LEADERS (TL), CO-IS, AND KEY PERSONS (KP)

Position	Name	Affiliation	e-mail
PI	**Orsini, Stefano**	INAF, Istituto di Fisica dello Spazio Interplanetario (IFSI) Via del Fosso del Cavaliere, 100 I-00133 Roma, Italy Phone: +39 0649934612 Phone (PO): +39 06 49934386 Fax: +39 0649934383	stefano.orsini@ifsi-roma.inaf.it
TL Project Scientist	**Hilchenbach, Martin**	MPS, Max-Planck-Institut für Sonnensystemforschung, Max Planck Str. 2, 37191 Katlenburg-Lindau, Germany Phone: +49 55 56 97 91 62	hilchenbach@mps.mpg.de
TL Project Scientist	**Hsieh, Ke Chiang**	University of Arizona, Department of Physics Tucson, AZ 85721, USA Phone: +01 520 621 6772	hsieh@physics.arizona.edu
TL Project Manager	**Di Lellis, Andrea Maria**	AMDL S.r.l., Via Giovanni Angelini 33, 00149 Roma, Italy PM Project Office: Phone: +39 49934558 Mobile: +39338.9699199 Fax: +39 06.49934383	amdl@iasf-roma.inaf.it
TL Project Office	**Mura, Alessandro**	Inaf, Istituto di Fisica dello Spazio Interplanetario (IFSI) Via del Fosso del Cavaliere, 100 I-00133 Roma, Italy Phone: +39 0649934386 Fax: +39 0649934383	alessandro.mura@ifsi-roma.inaf.it
TL, Leading Co-I	**Rifai Habbal, Shadia**	Institute for Astronomy, University of Hawaii, Honolulu, HI 96822, USA Phone: +01 520 621 6772	shadia@ifa.hawaii.edu
Leading Co-I H/W provider	**Wurz, Peter**	Physikalisches Institut University of Bern Sidlerstrasse 5 CH-3012 Bern, Switzerland Phone: +41 31 631 44 26 Fax: +41 31 631 4405	peter.wurz@space.unibe.ch
Leading Co-I H/W provider	**Dandouras, Iannis**	Centre d'Etude Spatiale des Rayonnements 9, Avenue du Colonel Roche 31028 Toulouse Cedex 4, France Phone:+33(0)561556676 Fax:+33(0)561556701	iannis.dandouras@cesr.fr

Leading Co-I H/W provider	**Kallio, Esa**	Finnish Meteorological Institute (FMI) Space Research Unit P.O.BOX 503, FIN-00101 Helsinki, Finland Phone: +358 9 1929 4636 Fax: +358 9 1929 4603	esa.kallio@fmi.fi
Leading Co-I H/W provider	**Czechowski, Andrzej**	Space Research Centre, Polish Academy of Sciences, Bartycka 18A, PL 00-716 Warsaw, Poland: Phone: +48 22 403766	ace@cbk.waw.pl
KP	**Aoustin, Claude**	Centre d'Etude Spatiale des Rayonnements 9, Avenue du Colonel Roche 31028 Toulouse Cedex 4, France	aoustin@cesr.fr
Co-I	**Bamert, Karin**	Physikalisches Institut University of Bern Sidlerstrasse 5 CH-3012 Bern, Switzerland	karin.bamert@soho.unibe.ch
Co-I	**Berrilli, Francesco**	Physics Department, University of Rome Tor Vergata, Viale della Rcerca Scientifica, 1I-00133 Roma, Italy	berrilli@roma2.infn.it
Co-I	**Bruno, Roberto**	Inaf, Istituto di Fisica dello Spazio Interplanetario (IFSI) Via del Fosso del Cavaliere, 100 I-00133 Roma, Italy	roberto.bruno@ifsi-roma.inaf.it
Co-I	**Collier, Michael R.**	NASA Goddard Space Flight Center Greenbelt, Maryland 20771	michael.r.collier@nasa.gov
Co-I	**Daglis, Ioannis**	Institute Space Applications Remote Sensing / National Observatory of Athens, Metaxa and Vas. Pavlou Str. 15236 P.Penteli, Greece	daglis@space.noa.gr
Co-I	**D'Amicis, Raffaella**	Inaf, Istituto di Fisica dello Spazio Interplanetario (IFSI) Via del Fosso del Cavaliere, 100 I-00133 Roma, Italy	raffaella.damicis@ifsi-roma.inaf.it
KP	**De Angelis Elisabetta**	Istituto di Fisica dello Spazio Interplanetario (IFSI) Via del Fosso del Cavaliere, 100 I-00133 Roma, Italy	deangelis@ifsi-roma.inaf.it
Co-I	**Esser, Ruth**	Department of Physics, The Auroral Observatory, Faculty of Science, University of Tromsø, N-9037 Tromsø, Norway	ruth.esser@phys.uit.no
Co-I	**Giacalone, Joe**	University of Arizona, Lunar & PLanetary Lab., Tucson, AZ 85721, USA	giacalon@lpl.arizona.edu

Co-I	**Gruntman, Mike**	Astronautics and Space Technology Division Viterbi School of Engineering, MC-1192 University of Southern California Los Angeles, California 90089-1192	mikeg@usc.edu
Co-I	**Ho, George**	Johns Hopkins University Applied Physics Laboratory (JHU/APL) 11100 Johns Hopkins Road, Laurel, MD 20723, USA	george.ho@jhuapl.edu
Co-I	**Kota, Jozsef**	Lunar and Planetary Laboratory, University of Arizona, Tucson, AZ, 85721, USA	kota@lpl.arizona.edu
KP	**Kucharek, Harald**	Space Science Center & Department of Physics, University of New Hampshire, Durham, NH03824, USA	harald.kucharek@unh.edu
Co-I	**Leoni, Roberto**	Istituto di Fotonica e Nanotecnologie/CNR Via Cineto Romano 42 00156 Roma – Italy	roberto@ifn.cnr.it
Co-I	**Livi, Stefano**	Southwest Research Institute 6220 Culebra Road San Antonio, TX 78228 210-522-3310	stefano.livi@swri.edu
Co-I	**Mann, Ingrid**	Department of Earth and Planetary Science, Faculty of Science, Kobe University, Nada, Kobe 657-8501, Japan	mann@diamond.kobe-u.ac.jp
Co-I	**Marsch, Eckart**	MPS, Max-Planck-Institut für Sonnensystemforschung, Max Planck Str. 2, 37191 Katlenburg-Lindau, Germany	marsch@linmpi.mpg.de
Co-I	**Massetti, Stefano**	Istituto di Fisica dello Spazio Interplanetario (IFSI) Via del Fosso del Cavaliere, 100 I-00133 Roma, Italy	stefano.massetti@ifsi-roma.inaf.it
KP	**Medale, Jean-Louis**	Centre d'Etude Spatiale des Rayonnements 9, Avenue du Colonel Roche 31028 Toulouse Cedex 4, France	louis.medale@cesr.fr
Co-I	**Möbius, Eberhard**	Space Science Center & Department of Physics, University of New Hampshire, Durham, NH03824, USA	eberhard.moebius@unh.edu
KP	**Nowosielski, Witold**	Space Research Centre, Polish Academy of Sciences, Bartycka 18A, PL 00-716 Warsaw, Poland	witnow@cbk.waw.pl
Co-I	**Orfei, Renato**	Istituto di Fisica dello Spazio Interplanetario (IFSI) Via del Fosso del Cavaliere, 100 I-00133 Roma, Italy	renato.orfei@ifsi-roma.inaf.it

KP	**Orleanski, Piotr**	Space Research Centre, Polish Academy of Sciences, Bartycka 18A, PL 00-716 Warsaw, Poland	porlean@cbk.waw.pl
KP	**Scheer, Jürgen**	Physikalisches Institut University of Bern Sidlerstrasse 5 CH-3012 Bern, Switzerland	jscheer@space.unibe.ch
KP	**Schmidt, Walter**	Finnish Meteorological Institute Space Research Unit P.O.Box 503 FIN-00101 Helsinki - Finland	walter.schmidt@fmi.fi
Co-I	**Selci, Stefano**	Istituto Sistemi Complessi/CNR, Via del Fosso del Cavaliere, 100 I-00133 Roma, Italy	stefano.selci@isc.cnr.it
Co-I	**Storini, Marisa**	Istituto di Fisica dello Spazio Interplanetario (IFSI) Via del Fosso del Cavaliere, 100 I-00133 Roma, Italy	marisa.storini@ifsi-roma.inaf.it
Co-I	**Zurbuchen, Thomas H.**	Dept. of Atmospheric, Oceanic, and Space Sciences University of Michigan, USA	thomasz@umich.edu

Associated Institutions (with names of all participants)

LEADING FUNDING AGENCY:

- **Italian Space Agency (ASI, Agenzia Spaziale Italiana), Viale Liegi 26, 00198, Roma, Italy.**

Lead Funding Agency	Contact person	address	e-mail
ASI	**Simona Di Pippo, Enrico Flamini**	**Unità Osservazione dell'Universo Agenzia Spaziale Italiana Viale Liegi 26, 00198, Roma, Italy Tel. +39 06 85671 Fax. +39 06 85671**	**dipippo@asi.it flamini@asi.it**

PI INSTITUTE

- **Istituto di Fisica dello spazio Interplanetario IFSI / INAF, Via Fosso del Cavaliere 100, 00133 Roma, Italy**
  Stefano Orsini, Dr Roberto Bruno, Raffaella D'Amicis, Elisabetta De Angelis, Stefano Massetti, Alessandro Mura, Renato Orfei, Christina Plainaki, Nello Vertolli

HARDWARE PROVIDING INSTITUTION (FUNDED INDIPENDENTLY)

- **Physikalisches Institut, Space Research & Planetary Sciences, Sidlerstrasse 5, CH - 3012 Bern, Switzerland**
  Peter Wurz, Jurgen Scheer, Karin Bamert
- **Centre d'Etude Spatiale des Rayonnements CESR, 9, av du Colonel Roche, 31028 Toulouse cedex 4, France (funded by CNES)**
  Iannis Dandouras, Claude Aoustin, Jean-Louis Medale, Philippe Louarn

- **Finnish Meteorological Institute, Erik Palménin aukio, FI-00560 HELSINKI, Finland**
  Esa Kallio, Walter Schmidt
- **Space Research Centre, Bartycka 18 A, 00-716 Warsaw, Poland**
  Andrzej Czechowski, Maciej Bzowski, Piotr Orleanski, Witold Nowosielski

OTHER ASSOCIATED INSTITUTIONS (WITH NAMES OF ALL PARTICIPANTS)

Europe:

- **AMDL s.r.l.,** v.le Somalia 133, 00199 Roma, Italy
  Andrea M. Di Lellis
- **Istituto di Fotonica e Nanotecnologie (IFN), CNR, via Cineto Romano 42, 00156 Roma, Italy**
  Roberto Leoni
- **Istituto dei Sistemi Complessi (ISC), CNR, Via Fosso del Cavaliere 100, 00133 Roma, Italy**
  Stefano Selci
- **Dipartimento di Fisica, Università di Roma 2 – Tor Vergata, 00133 Roma, Italy**
  Francesco Berrilli, Dario Del Moro, Silvia Giordano, Valentina Penza
- **Max-Planck-Institut für Sonnensystemforschung, Max-Planck-Str. 2, 37191 Katlenburg-Lindau, Germany**
  Martin Hilchenbach, Eckart Marsch, Joachim Woch
- **Department of Physics, The Auroral Observatory, Faculty of Science, University of Tromsø, N-9037 Tromsø, Norway**
  Ruth Esser
- **Institute for Space Applications & Remote Sensing, National Observatory of Athens**
  Athens, Greece
  Ioannis A. Daglis

Japan:

- **Department of Earth and Planetary Science, Faculty of Science, Kobe University, Nada, Kobe 657-8501, Japan**
  Ingrid Mann

US:

- **University of Arizona, Tucson, AZ 85721, USA**
  Department of Physics: Ke Chiang Hsieh
  Lunar & Planetary Laboratory: J. Randy Jokipii, Joe Giacalone, Jozsef Kota
- **University of Hawaii, Institute for Astronomy, 2680 Woodlawn Drive, Honolulu, HI 96822, USA**
  Shadia Rifai Habbal
- **Southwest Research Institute, San Antonio, TX 78228, San Antonio, TX, USA**
  Stefano Livi
- **JHU/APL, MP3 E132 11100 Johns Hopkins Road, Laurel, MD 20723, USA**
  George Ho

- **Experimental Space Plasma Group, University of New Hampshire, Durham NH 03824, USA**
  Eberhard Möbius**,** Harald Kucharek
- **Astronautics and Space Technology Division, Viterbi School of Engineering, 854 Downey Way, RRB-224, MC 1192, University of Southern California, Los Angeles, CA 90089-1192, USA**
  Mike Gruntman
- **Department of Atmospheric, Oceanic and Space Sciences, The University of Michigan, Space Research Building, Ann Arbor, MI 48109-2143, USA**
  Thomas H. Zurbuchen
- **Interplanetary Physics, NASA/Goddard Space Flight Center, Greenbelt, Maryland 20771, USA**
  Michael R. Collier

E-MAIL LIST:

Europe:

flamini@asi.it, dipippo@asi.it, stefano.orsini@ifsi-roma.inaf.it, roberto.bruno@ifsi-roma.inaf.it, raffaella.damicis@ifsi-roma.inaf.it, elisabetta.deangelis@ifsi-roma.inaf.it, stefano.massetti@ifsi-roma.inaf.it, anna.milillo@ifsi-roma.inaf.it, alessandro.mura@ifsi-roma.inaf.it, renato.orfei@ifsi-roma.inaf.it, marisa.storini@ifsi-roma.inaf.it, nello.vertolli@ifsi-roma.inaf.it, amdl@iasf-roma.inaf.it, berrilli@roma2.infn.it, delmoro@roma2.infn.it, giordano@roma2.infn.it, penza@roma2.infn.it, roberto@ifn.cnr.it, francesco.mattioli@ifn.cnr.it, stefano.selci@isc.cnr.it, hilchenbach@mps.mpg.de, marsch@linmpi.mpg.de, woch@linmpi.mpg.de, esa.kallio@fmi.fi, walter.schmidt@fmi.fi, peter.wurz@phim.unibe.ch, karin.bamert@soho.unibe.ch, jscheer@space.unibe.ch, ace@cbk.waw.pl, bzowski@cbk.waw.pl, porlean@cbk.waw.pl, witnow@cbk.waw.pl, iannis.dandouras@cesr.fr, aoustin@cesr.fr, jean-louis.medale@cesr.fr, philippe.louarn@cesr.fr, szego@rmki.kfki.hu, ruth.esser@phys.uit.no

Japan:

mann@diamond.kobe-u.ac.jp

US:

hsieh@physics.arizona.edu, jokipii@lpl.arizona.edu, giacalon@lpl.arizona.edu, kota@lpl.arizona.edu, shadia@ifa.hawaii.edu, stefano.livi@swri.edu, george.ho@jhuapl.edu, eberhard.moebius@unh.edu, harald.kucharek@unh.edu, mikeg@usc.edu, thomasz@umich.edu, michael.r.collier@nasa.gov

FTP ADDRESS AT WHICH THE PROPOSAL CAN BE FOUND AT ELECTRONIC FORM:
site: ftp.artov.rm.cnr.it
username: scenario
password: nswd

Executive Summary

I. Proposal Objectives and Compliance with SolO Sci-RD

The proposed NSWD - SCENARIO (Neutral Solar Wind Detector - Solar Corona ENA Radiation Imagine Observer) will detect and characterize the neutral component of the solar wind in the inner heliosphere for the first time. The proposed observation will directly contribute to three of the four scientific goals of the Solar Orbiter presented in the Announcement of Opportunity:

- *Determine the properties, dynamics and interactions of plasma, fields and particles in the near-Sun heliosphere;*
- *Investigate the links between the solar surface, corona and inner heliosphere;*
- *Explore, at all latitudes, the energetics, dynamics and fine-scale structure of the Sun's magnetized atmosphere.*

In order to fulfil the listed tasks, *in situ* analysis of the solar wind electron and ion populations is not sufficient; hence, we propose this further investigation of the solar wind 'zero-charge state', as a fundamental tracer for understanding the solar wind evolution from the corona to the spacecraft vantage point. Furthermore, the solar wind neutral component travels unperturbed along tens of solar radii, preserving the same properties of the solar wind at the generation point. Hence, this signal will yield important clues about the way the solar wind evolves with heliocentric distance from the Sun: such properties may be derived from the detection of the neutral solar wind at the Solar Orbiter location. Given the strong complementarity between SCENARIO and Solar Wind Analyzer (SWA) instrument in investigating the solar wind expansion and the environmental effects on its dynamics, we strongly request that SCENARIO could be eventually integrated in the SWA package. This merging is also suitable for an essential system resource saving: basically SCENARIO is a particle instrument operating in the same energy ranges as all SWA analyzers, hence it looks natural to include SCENARIO within this package by sharing a common DPU system.

II. SCENARIO Scientific Objectives

- **Radial evolution of solar wind structures in the inner heliosphere**

The SWA *in situ* measurements will allow estimates of solar wind (SW) evolution from a single vantage point, hence, only mixed temporal evolution will be monitored (or a mixture of temporal and spatial evolution during the non corotational phase), at a given distance from the Sun, with the goal to '... *provide observational constraints on kinetic plasma properties for a fundamental and detailed theoretical treatment of all aspects of coronal heating*'. A crucial and fruitful complement to such measurements would come from SCENARIO SW remote sensing capability, which will give a concrete chance to expand our knowledge about SW evolution (flux intensity, energy and temperature) by means of multi-point analysis along the SW expansion path.

- **Influence of CMEs on the structure of the inner heliosphere**

Continuous measurements of the Neutral Solar Wind (NSW) will open a possibility to directly study the dynamics of major transient processes in otherwise inaccessible regions of propagating coronal mass ejections (CMEs). Indeed, SCENARIO will be able to observe a critical part of the energy distribution that will determine whether suprathermal tails exist in the distribution close to the Sun (15÷20 R_S) during quiet times, or just during CME events.

- **Solar wind microstate evolution with radial distance**

The capability of SCENARIO to detect neutral atoms coming from below 20 R_S represents an unique possibility to access to information about the kinetic state of the plasma below the Alfvén radius. This distance is also crucial for discriminating between Alfvénic turbulence propagating modes, since MHD turbulence is completely different moving across this radius.

- **Acceleration and heating mechanisms that lead to coronal hole –associated fast solar wind**

Remote sensing via SCENARIO measurements will allow determining spatial evolution of fast solar wind along its path inside the inner heliosphere. Thus, parallel temperature profiles versus radial distance, when compared to both SWA *in situ* measurements and coronograph data (which will be effective in perpendicular temperature estimates, see D'Amicis et al., 2007), will provide useful information on both fast streams acceleration and heating mechanisms.

- **Sources of slow solar wind, and what is its temporal and spatial evolution**

Similarly, remote sensing slow solar wind via SCENARIO measurements will allow determination of dynamics along its path inside the inner heliosphere. Hence, if SWA measurement will provide

information about the location of slow solar wind sources (taking profit of the time-varying S/C position relative to Sun surface), SCENARIO will consistently support investigations about its spatial evolution.

- **Sources and the global dynamics of eruptive events (CMEs) and what are their effects on the inner heliosphere**

This objective may be studied by combining remote sensing the early stage of CME in UV by the coronograph on SolO and optical observations on Earth, and *in situ* measurement of energetic particles accelerated by the CME-driven shock by SWA and particle detectors located on Solar Orbiter as well as Solar Sentinels. To reach a fuller understanding of this propagating and expanding phenomenon, however, SCENARIO data will be crucial, because only direct sampling of the CME-associated ion population via ENA can we discern the evolution of the shock before it passes by the *in situ* particle detectors.

- **Nature of coronal hole boundaries, how do they evolve and how do they project into the inner heliosphere**

The evolution of SW shock boundaries is usually monitored by *in situ* plasma measurements, taking advantage of spacecraft motion and/or temporal variations; nevertheless, only one point in space. SCENARIO, on the other hand, by measuring plasma at a given distance via ENA, will permit a third kind of investigation of the temporal development of coronal hole boundaries. In fact, the angular resolution of the neutral flux can yield information about the solar wind properties at different distances. Hence, thanks to the NSW flow direction angular scanning, possible locations of SW regimes upstream as well as downstream the shock boundary will be monitored at the same time.

Other Scientific Objectives are: ***In situ*** **characterization of the Solar Wind; Distribution and intensity of the inner source ENA radiation from other heliospheric sources**

III. Required performances of the SCENARIO experiment

Summary table for Scientific Performance Requirements

Scientific Objective	Expected flux (cm^{-2} s^{-1})	Energy range (keV)	Energy resolution (dE/E)	Minimum FOV (°)	Angular resolution (°)	Time resolution (m)
Radial evolution of solar wind structures in the inner heliosphere	$10^3 \div 10^4$	0.5 ÷ 2	25 %	~10×10	~2	≤60
Influence of CMEs on the structure of the inner heliosphere	$10^3 \div 10^6$	1÷5	25 %	~5×5	~1	≤10
Solar wind microstate evolution with radial distance	10^3	0.5 ÷ 2	25 %	~10×10	~2	≤60
Acceleration and heating mechanisms that lead to coronal hole –associated fast solar wind	10^3	1 ÷ 5	25 %	~5×5	~1	≤60
Sources of slow solar wind, and what is its temporal and spatial evolution	10^4	0.5 ÷ 2	25 %	~10×10	~2	≤60
Sources and the global dynamics of eruptive events (CMEs) and what are their effects on the inner heliosphere	$10^3 \div 10^6$	2 ÷ 5	25 %	~5×5	~1	≤60
Nature of coronal hole boundaries, how do they evolve and how do they project into the inner heliosphere	10^3	0.5 ÷ 2	25 %	~5×5	~1	≤60
In situ **characterization of the Solar Wind**	10^4	0.5 ÷ 5	25 %	N/A	N/A	≤60
Distribution and intensity of the inner source	10^4	0.5 ÷ 2	25 %	~10×10	~2	≤60
ENA radiation from other heliospheric sources	N/A	0.5 ÷ 5	25 %	N/A	N/A	N/A

IV. Experiment operations and scientific analysis

The nominal operational modes of SCENARIO are based on automatic procedures, which do not require any specific assistance. Mode of operation changes may be necessary at times during in-orbit phases. The SCENARIO team will support the Mission Operation Centre (MOC) and Science Operation Centre (SOC) as required.

Science operations will be conducted in close coordination with SOC. The PI will receive the raw data and the instrument and spacecraft housekeeping from MOC and will distribute them to the Co-PIs and

Co-Is. Reduction of science data is under the responsibility of the team. The SCENARIO science management plan will comply the science operation plans, the data handling and archiving concepts as defined by the SOC. After proprietary period of 6 months, the data will be delivered to the SolO scientific archive for public domain within the other SolO scientists and the whole scientific community

V. Summary of Required Spacecraft Resources

UNIT	MASS (g)	POWER (W)	TELEMETRY (b/s)
SCENARIO (inclusive of SCU)	1559 (including contingency)	6 (on primary bus)	100

VI. Management Scheme

Major Responsibilities: Team leaders

Principal Investigator	Stefano Orsini	IFSI/INAF, Roma, Italy
Project Scientist	Martin Hilchenbach	MPS, Katlenburg-Lindau, Germany
Project Scientist	Ke Chiang Hsieh	University of Arizona, Tucson, AZ, USA
Project and Program Manager	Andrea M. Di Lellis	AMDL, Roma, Italy
US Team Leading Co-I	Shadia Rifai Habbal	Inst. Astronomy, Uni. of Hawaii, USA
PI Project Office	Alessandro Mura	IFSI/INAF, Roma, Italy

Hardware Providers Table:

Team Institutions	Role	Delivery Responsibility
IFSI/INAF (supported by AMDL, IFN, ISC)	PI	Sensor Responsibility
CESR, Toulouse, France	Co-I	High Voltages
Physikalisches Institut, Bern, Switzerland	Co-I	Ionizing surfaces, Calibration
FMI, Helsinki, Finland	Co-I	Scientific EGSE
Space Research Centre, Warsaw, Poland	Co-I	Low DC/DC power supply, supporting activity for post delivery integration & test

Science Team:

Shadia Rifai Habbal **(US Team Leader)**, Ke Chiang Hsieh, Martin Hilchenbach, Andrzej Czechowski, R. D'Amicis, A. Mura, R. Bruno, Maciej Bzowski, Joe Giacalone, J. R. Jokipii. Jozsef Kóta, Mike Gruntman, Harald Kucharek

Instrument Design Support:
Michael R. Collier, Iannis Dandouras, Mike Gruntman, Esa Kallio, Martin Hilchenbach, Jean-Louis Medale, Ke Chiang Hsieh, Stefano Livi, Eberhard Möbius, Peter Wurz, Harald Kucharek

Technical Support
Nello Vertolli, Piotr Orleanski, Witold Nowosielski

VII. Summary of Financial Status

All necessary endorsement letters by ASI and other h/w providing institutions (Uni. of Bern, CNES/CESR, FMI, PAS/SRC) have been regularly delivered and included in the financial plan document SO-NSWD-PL006-001-1

VIII. Possible departure from the Constrains stated in the PSD

N/A

IX. Requirements imposed on other instruments or spacecraft subsystem

N/A

X. Annex: Experiment data sheet

	Parameter	Units	Value/Description	Remarks
General	Reference P/L	NSWD	SO-NSW-RS-002	EIDB
	Type of optics	N/A	Pin Hole	
	Type of camera	N/A	TOF Chamber	Time shuttered
Instrument optics	Aperture (longest dim)	mm	25	Rectangular aperture of 10x25 mm^2
	Focal length	mm	130	TOF length
	Focal number	N/A	N/A	
	Field of view		12° × 5°	12° along orbital plane
	Pixel IFOV		1° × 5°	
	Spectral range	keV	0.1 ÷ 5	
	Filter bandwidth	nm	N/A	
	Energy/ToF Channels	#	16÷128	Nominal mode
	Geom. Factor	cm^2	2×10^{-3}	
	Geom. Factor	cm^2 sr	4×10^{-5}	
	Dynamic range	cts/ cm^2 sr*keV	$10^3 \div 10^7$	
Instrument performances	Pixel lines	#	16	used for Energy
	Pixels per line	#	8	used for Azimuth in low angular resolution, when not operating the grid scanning.
	Pixel pitch	m	1500	
	Peak quantum efficiency	%	>50%	E.g. Burle 'Long Life' MCPs
	Exposure time	s	60	
Instrument resolution	Energy resolution	dE/E	25%	
	Angular resolution	μrad/px	1500	
Instrument physical properties	Mass, total (protection baffle NOT included)	g	1559	Including 20% Cont., (excluding DPU hopefully provided by SWA package)
	Mass, optics	g	339.7	
	Mass, box	g	556.3	
	Mass, electronics	g	600	
	Dimension (box)	mm^3	200 × 115 × 75	
	Baffle length	cm	7.5	Shadowing direct solar view.
Instrument power requirements	Average power	W	6.6	On Primary (DC-DC 75% efficiency)
	Installed Heater Power	W	N/A	
Instrument Data requirements	Time/imaging sequence	s	60	Science Mode: Nominal Mode
	Data rate to Orbiter OBDH	bps	50+50	Science Mode: Nominal Mode, 12 Pix × 16 Ene_chs × 16 bit / 60 s + HK & Conting: 50 b/s+50 b/s

TABLE OF CONTENTS

1. SCIENTIFIC OBJECTIVES AND CAPABILITIES 3
1.1 Introduction 3
1.2 Sources of ENAs 4
1.2.1 Intrinsic neutral solar wind 4
1.2.2 Neutral solar wind from charge exchange with the gas in the heliosphere 5
1.2.3 ENAs from seed particles for SEP in CME 6
1.3 Dynamics and Structure of the Solar Wind: Simulations of the NSW at 48 R_S 7
1.3.1 Coronal neutral hydrogen 8
1.3.1.1. Models for fast solar wind neutrals 8
1.3.1.2. Models for slow solar wind neutrals 10
1.3.2. Models of the inner source neutral hydrogen 11
1.3.3 Models for neutral solar wind helium 12
1.4 SCENARIO Scientific Objectives 13
1.4.1 Summary of expected NSW signal intensities 14
1.4.2 Primary Scientific Objectives 14
1.4.2.1 Objectives related to SolO PDD point: “Determine the properties, dynamics and interactions of plasma, fields and particles in the near-Sun heliosphere” 15
1.4.2.2 Objectives related to SolO PDD point: “Investigate the links between the solar surface, corona and inner heliosphere” 15
1.4.2.3 Objectives related to SolO PDD point: “Explore, at all latitudes, the energetics, dynamics and fine-scale structure of the Sun’s magnetized atmosphere” 16
1.4.3 Other Scientific Objectives 16
1.4.4 Summary 17
Appendix 1: Simulations details 18
References 20

2 TECHNICAL DESCRIPTIONS AND DESIGN 22
2.1 Introduction 22
2.2 Instrument Design Elements including their design maturity 22
2.4 Expected Geometrical Factor 26
2.3 Maturity of the design 26
2.5 Accommodation 27

3 INSTRUMENT PERFORMANCE 28
3.1 SCENARIO Characteristics 28
3.2 ENA measurement concepts 28
3.3 Simulation of expected signal 29
References 30

4 SUMMARY OF INSTRUMENT INTERFACES 31
4.1 SCENARIO Mass Budget 31
4.2 SCENARIO Power Budget 32
4.3 SCENARIO Telemetry Budget 33

5 TEST AND CALIBRATION PLAN 34
5.1 Modelling 34
5.2 Ground Testing and Calibration 34
5.3 In-flight Calibration 34

6. SYSTEM LEVEL ASSEMBLY, INTEGRATION AND VERIFICATION.....34
6.1 Requirements 34
6.2 Deliverable Models.....34
6.3 System Level Testing.....35
7 FLIGHT OPERATIONS CONCEPT 35
7.1 Normal operations.....35
7.2 Other modes 36
7.2.1 Calibration mode.....36
8 DATA REDUCTION AND SCIENTIFIC ANALYSIS PLANS 36
8.1 Data Processing and Standard Data Products.....36
8.2 Specific Software Products.....37
8.3 Software Product and Procedure Standards.....37
8.4 Compliance with Science Data Policy defined in SolO Science Management Plan 37
9 PROGRAMMATIC 38
10 Annex 1: 38
10.1 Qualifications and Experience of PI Team and Key Staff.....38

1. SCIENTIFIC OBJECTIVES AND CAPABILITIES

1.1 Introduction

The proposed Neutral Solar Wind Detector (NSWD) is named SCENARIO (Solar Corona ENA Radiation Imagine Observer). In the following, we will describe the way it can directly contribute to three of four scientific goals of the Solar Orbiter (SolO) presented in the Announcement of Opportunity:

- **Determine the properties, dynamics and interactions of plasma, fields and particles in the near-Sun heliosphere;**
- **Investigate the links between the solar surface, corona and inner heliosphere;**
- **Explore, at all latitudes, the energetics, dynamics and fine-scale structure of the Sun's magnetized atmosphere.**

While SolO's baseline optical instruments can *remotely sense* the plasma in the base region where coronal heating and particle acceleration occur, and SolO's baseline plasma and particle instruments can monitor *in situ* the flux of already accelerated ions and electrons, the *direct sampling of the particles in the base region*, where they are being heated and accelerated, however, can only be done through remote sensing of the charged particle populations while being heated and accelerated, *via* energetic-neutral-atom (ENA) imaging. ENA imaging (Hsieh *et al.*, 1992; Gruntman, 1997, Wurz, 2000) has matured and proven successful in the study of heliospheric and planetary energetic ion populations (*e.g.*, Hilchenbach *et al*., 1998; Collier *et al*., 2001; Mitchell *et al*., 2001; Brinkfeldt *et al*., 2006, Barabash *et al*., 2007, and review by Orsini *et al*. 2008). This is because 1) ENAs are energetic ions neutralized by charge exchange with ambient neutral atoms, such as coronal HI, interstellar HeI, and desorbed gas from interstellar dust, or through penetration of interplanetary dust (Wimmer-Schweingruber and Bochsler, 2003) in the inner heliosphere; 2) these neutral particles are unaffected by electric and magnetic fields along their ballistic trajectories between the sites of neutralization and detection. Thus, ENA imaging is analogous to photographing with photons.

Aiming at the stated scientific goals, responding to the call of High Priority Augmentations to the Solar Orbiter Baseline Mission (Section 3.1.1 of AO), and taking advantage of our cumulative expertise and our new innovative technique in ENA imaging, we propose the NSWD:SCENARIO for the Solar Orbiter mission.

In Section 1.2, we shall:

1) identify the ENA sources within the field of view of SCENARIO along the orbit of SolO;

2) point to the important spatial and temporal information which can be obtained

through ENAs on the dynamics and structure of the solar wind (SW) and on the solar energetic particles (SEP) that are accelerated in solar events, such as coronal mass ejections (CMEs).

In essence, ENAs complement the *in situ* measurements of the solar wind analyzer (SWA) and energetic particle packages by providing i) remote sensing of the ionized solar wind component and at the same time ii) *in situ* characterization of the 'zero charge state' of the solar wind. In particular, we show that SCENARIO will yield important information for the understanding of solar wind heating and energetic particles acceleration during solar events, in regions otherwise inaccessible to *in situ* measurements.

In Section 1.3, we shall present the expected SCENARIO observations at the orbit of SolO according to simulations of the signal on the basis of existing solar wind models. Because of the lack of models for the seed particles for SEP, any resulting simulation would be inherently weak and can only be constrained by the new SolO observations.

In Section 1.4, we will list and comment on the SCENARIO Scientific Objectives.

1.2 Sources of ENAs

1.2.1 Intrinsic neutral solar wind

The properties of the coronal plasma reflect the properties of the processes that control coronal heating and consequently the acceleration of the solar wind. Probing coronal plasmas is then tantamount to exploring these processes. Remote sensing observations, through imaging in selected wavelength bandpasses and spectroscopy, are currently the only tools available. Despite the most recent high spatial and temporal observations, such as from the HINODE mission (Science, vol. 318, 2007), model studies remain essential for probing these processes. However, protons, the dominant component of the coronal plasma, do not have a direct spectroscopic signature. Lyα coronal emission, discovered during the total solar eclipse of 1970 (Gabriel *et al.,* 1971), revealed the presence of neutral hydrogen in the corona, and thus provided the first proxy to infer properties of coronal protons through charge exchange. This has been demonstrated theoretically (Olsen *et al.,* 1994; Allen *et al.*, 1998, 2000) and observationally (Withbroe *et al.*, 1982; Kohl *et al.*, 1995). The radial distance beyond which the coupling between neutrals and protons ceases to be significant depends on coronal conditions (see review by Fahr *et al.*, 2007, and models by Olsen *et al.*, 1994 and Allen *et al.*, 1998, 2000). However, once decoupled, the neutral hydrogen atoms preserve the imprint of protons in the corona from their last encounter. Contrary to charged particles, neutrals can travel long distances on ballistic trajectories, oblivious to the solar magnetic field, only subject to reliably quantifiable losses. Hence, measurements of the three-dimensional velocity distribution of neutral hydrogen by SCENARIO on SolO would yield information, for the first time, about protons in the acceleration region of the solar wind whose imprints have been frozen into the neutrals, the *intrinsic neutral solar wind* (NSW).

According to the actual knowledge (see D'Amicis et al., 2007, and reference therein), the NSW decouples from the ionized component in the inner heliosphere, at heliocentric distances <20 R_S (solar radii). This range is particularly important, since it represents the distance at which the corona stops co-rotating with the surface of the Sun and the solar wind becomes super-Alfvénic. Using Helios *in situ* observations, this distance was at first evaluated and set between 10 and 30 R_S by Pizzo *et al*. (1983) and Marsch and Richter (1984). This distance also acts as a filter for the Alfvénic turbulence since only outward propagating modes will be able to escape from the Sun. Inward modes, being faster than the wind bulk speed, will precipitate back to the Sun if they are generated before this point (see ample literature reported in Bruno and Carbone, 2005). Thus, MHD turbulence is completely different moving across the Alfvén radius. Access to information about the kinetic state of the plasma below 20 R_S through the neutral solar wind and comparison with *in situ* plasma measurements would be extremely valuable for understanding wave-particle processes which are fundamental for solar wind heating and acceleration.

1.2.2 Neutral solar wind from charge exchange with the gas in the heliosphere

Energetic neutral atoms can also come from solar-wind protons and alpha particles after charge exchange with slow-moving neutral atoms and particles in the inner heliosphere, which do not belong to the solar wind. These ENAs are produced with the velocity distributions that reflect the distributions of the parent solar-wind protons or alpha-particles at the time and location of the charge-exchange process and can therefore be used for "remote imaging" of the solar wind plasma parameters in the corresponding source regions (Fahr *et al.,* 2007).

For observations towards the Sun, the charge exchange processes with the following neutral populations are important: 1) the inner source (see below) and 2) the inflowing interstellar gas penetrating to the vicinity of the Sun. The contribution from the interstellar gas in the outer heliosphere is small and can be neglected compared to other sources.

The inner source was discovered in the Ulysses/SWICS pick-up ion distributions (Geiss *et al.*, 1995; Gloeckler and Geiss, 1998). For the production of inner source ions the following processes have been proposed: 1) outgassing of the captured solar wind ions from dust grains, 2) sputtering of dust material, 3) passage of solar wind through small dust grains and their charge exchange, 4) collisional vaporization of dust and 5) the release of material from Sun-grazing comets. Only the first three mechanisms can provide the inner source pick up ions with the abundance ratios close to the solar wind abundances, as suggested by data. Mechanisms 1) and 2) require, however, a much larger (by more than 2 orders of magnitude) geometrical cross section of the dust grains than predicted by models of the circumsolar dust cloud. Mechanism 3) requires a substantial number of small dust grains. Note that the predicted densities of the dust population near the Sun vary significantly and *in situ* measurements are very desirable, but presently are not available. Since charge exchange cross sections are well known, the production of the inner source pick-up ions is associated with the production of a branch of the neutral solar wind, the *inner-source neutral solar wind*. As solar wind ions also lose energy in interactions of type 3), a measurement of the energy spectrum

of the neutral solar wind will provide a unique tool to distinguish between the competing theoretical inner source models (Allegrini *et al.*, 2005; Wimmer-Schweingruber and Bochsler, 2003; Mann and Czechowski, 2005; Bochsler *et al.*, 2006).

The neutral hydrogen of interstellar origin, which fills most of the heliosphere, is strongly suppressed inside 1 AU due to ionization by solar UV radiation. On the other hand, neutral helium of interstellar origin (with densities of about 0.015 cm^{-3}), however, can survive and will likely dominate the number density of neutrals to about 0.05 AU from the Sun. Its spatial distribution is asymmetric, with the density enhanced in the wake of the Sun's motion in the interstellar medium forming the "helium cone" (Gruntman, 1994; Gruntman and Izmodenov; 2004, Michels *et al.*, 2002; Kuhn et al. 2007; Möbius *et al.*, 2004; 2006). Therefore, solar-wind ions exchanging charge with interstellar HeI may contribute significantly to the neutral solar wind.

Another important neutral component in the solar wind is helium. Solar-wind alpha particles constitute up to 5% of the solar-wind ion number density (Aellig et al., 2001). Although the helium flux is at least three orders of magnitude smaller than that of neutral hydrogen, HeI has been detected spectroscopically in the corona at around 9 R_S and within 0.5 R_S above the limb. The origin of this He flux can be solar, interstellar, and/or dust.

SolO will semi-synchronously orbit the Sun at distances as close as 0.22 AU. Such observational geometry offers a unique opportunity to separate spatial and temporal variations of the solar wind, thus allowing the separation of contributions from different sources of the neutral solar wind. For example, dust-produced neutrals are expected to concentrate near the ecliptic plane while ENAs from the heliospheric sheath beyond the termination shock would exhibit upwind-downwind (interstellar wind) asymmetry. Hence, combining the measurements of NSW with those of pickup ions and dust should allow one to constrain possible physics of outgassing and sputtering, to better evaluate the size distribution and density of the dust population(s) in the Sun's vicinity. Furthermore, the evaporation of an occasional Sun-grazing comet would result in injection of a large mass of neutral gas and dust in the Sun’s vicinity, providing temporarily an environment well known from cometary physics, but at much higher plasma temperatures and densities. Coordinated cometary watch would yield unprecedented observations of such events in the inner heliosphere.

1.2.3 ENAs from seed particles for SEP in CME

Continuous measurements of the neutral solar wind will enable the possibility to directly study the dynamics of major transient processes in otherwise inaccessible regions of propagating coronal mass ejections (CMEs). The current paradigm of solar-energetic particles (SEPs) is that they can be subdivided into two separate classes: those associated with solar flares, and those associated with CME-driven shock waves (Reames *et al.*, 1999). The origin of this two-class paradigm lies in the composition of SEPs. Solar-flare (or "impulsive") events often show high charge states, enhancements of heavy ions and electrons, and unusually large ratios of $^3He/^4He$. However the view of impulsive solar flares as solar sources of impulsive SEP events has not yet been convincingly supported by observations (Nitta et al., 2006). This means that the fact that impulsive solar flares at well connected regions always result in ^3He rich SEP events it

is not yet uncontested. Limited studies on the solar sources of impulsive SEP events (Kahler et al., 1987; Reames et al., 1988) failed to see a characteristic pattern of the associated solar flares; sometimes no solar flares were found. The issue becomes more complicated since SEP events are now more frequently associated with CMEs (Kahler et al., 2001; Yashiro et al., 2004) than previously shown (Kahler et al., 1985). Moreover, large, gradual events associated with CMEs, on the other hand, are usually proton rich. Recent observations (Mason *et al.*, 1999) often show a mixture of these two classes of events indicating that smaller, more frequent flare-related events populate the inner heliosphere and these particles are then accelerated by the CME later. SCENARIO will be able to observe a critical part of the energy distribution that will determine whether suprathermal tails exist in the distribution close to the Sun (15÷20 R_S) during quiet times, or just during CME events. Related to this is the timing of SEP events seen at Earth and their solar origin (e.g. Cohen *et al.*, 2001). SCENARIO will be able to discern between the CME (e.g. coronograph images) and the CME-driven shock (heated particle distributions), which will be ahead of it. By knowing the arrival times of SEPs and shock locations (as a function of time) near the Sun, we will gain valuable information about the time and place particle acceleration occurs, which then provide important information on the shock acceleration rate and, indirectly, about the properties of the magnetic field fluctuations near the Sun. The kinetics of plasma-gas interaction in CMEs can be then studied via observations of the NSW fluxes and their variations.

The study of acceleration and propagation of energetic charged particles under different plasma conditions remains a central topic in space physics. Observing the dynamic processes requires sensing of ion populations near the Sun. Sensing the energetic ion populations via ENA is a unique technique based on the charge exchange between energetic ions and interstellar neutral H and He atoms in and out of the heliosphere. The proposed Neutral Solar-Wind Detector, SCENARIO, is therefore the first attempt at an *in situ* probe of the pristine coronal plasma in its quiescent and dynamic states. It indeed provides an investigation into the origin of neutrals in the corona and solar wind.

1.3 Dynamics and Structure of the Solar Wind: Simulations of the NSW at 48 R_S

In the following sections, we estimate what the neutral solar wind detector SCENARIO would detect, by demonstrating the NSW flux expected features from both slow and fast solar wind at SolO's perihelion, 0.22 AU or 48 R_S from the Sun. For simplicity, we consider the case when SolO's orbital plane coincides with the ecliptic. Figure 1.1A illustrates the angular aberration in the detected flux due to the orbital velocity of SolO relative to the Sun. This particular illustration, not precisely to scale, shows a NSW atom coming from the sunward direction when SolO is at its perihelion, where $v_{s/c}$ is perpendicular to the Sun-SolO line. This aberration graciously allows SCENARIO to detect NSW atoms coming from the sunward direction without being blinded by sunlight by setting the centre line of SCENARIO's FOV (12° in the orbital plane × 5° out of the plane) at 15° west of the Sun-SolO line. In the following, we will discuss the properties of the ENA flux the Sun's rest reference frame (see Figure 1.1B, and Appendix of section 1), and in Section 3.2 we will show simulation of the detected signal, including aberration effects and instrumental features. Among the three components of NSW described in the previous sections, only the intrinsic or coronal

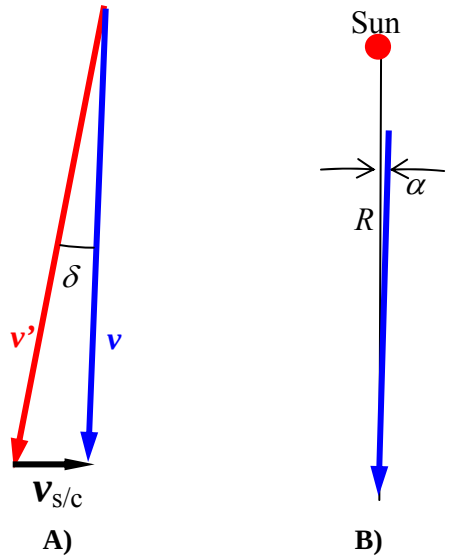

Figure 1.1. Panel A: actual particle direction of flight (v, in blue) and the apparent direction of arrival (v', in red). The s/c velocity ($v_{s/c}$, in black) causes an aberration effect (δ), allowing us to detecting ENAs from the sunward direction without exposing SCENARIO to direct sunlight. Panel B: viewing geometry in SolO's orbital plane; vantage point is at P; α is the azimuth angle, in the ecliptic plane, between the Sun-P direction and the direction actual of particle (blue vector, not to scale).

NSW and NSW produced by inner sources will be estimated. The lack of models for the third component, the seed particles for SEP in CME, would make any simulation weak. We hope new observations from SCENARIO will provide constraints on models of CME.

1.3.1 Coronal neutral hydrogen

To estimate the range of NSW fluxes to be measured by SolO at a perihelion distance of 48 R_S, an empirical model and a self-consistent model for the coronal/solar-wind plasma parameters (namely, velocity, temperature and density) for both fast and slow solar wind conditions are used. The empirical model, also referred to as 'reference' model, is based on coronal and *in situ* measurements (see references in D'Amicis *et al.,* 2007). As for the self-consistent solar wind models, the model by Allen *et al.* (2000) (referred to as 'Allen') is used for the fast solar wind, while the model by Lie-Svendsen *et al.* (2003) (referred to as 'Lie-Svendsen') with an expansion factor of f=1, is used for the slow solar wind. All these models address the loss mechanism for re-ionization of neutrals (charge exchange, photoionization, and collisions).

1.3.1.1. Models for fast solar wind neutrals

For the fast solar wind, the calculated flux, integrated over energy and angle (from 0.5 to 5 keV, and in a 10° solid angle cone centred around the central direction), is of the order of 4 10^3 cm^{-2} s^{-1} for both solar wind models. The differential flux in angle ($\partial\Phi/\partial\alpha$) (Fig. 1.2A; azimuth along the ecliptic plane, 0 = towards the Sun) shows that the signal is concentrated in a small region around the Sun direction. The width of this region depends on the solar wind model applied, and may be up to 10° for "Allen", while it is significantly sharper, a few degrees, for the "reference" model. Conversely, the differential fluxes at 0° are different, so that the fluxes, integrated over all angles, are quite the same.

Similarly, the energy differential flux ($\partial\Phi/\partial E$) (Fig. 1.2B) is peaked at about 2 keV for both models, being slightly smoother for the Allen model. These differences could be

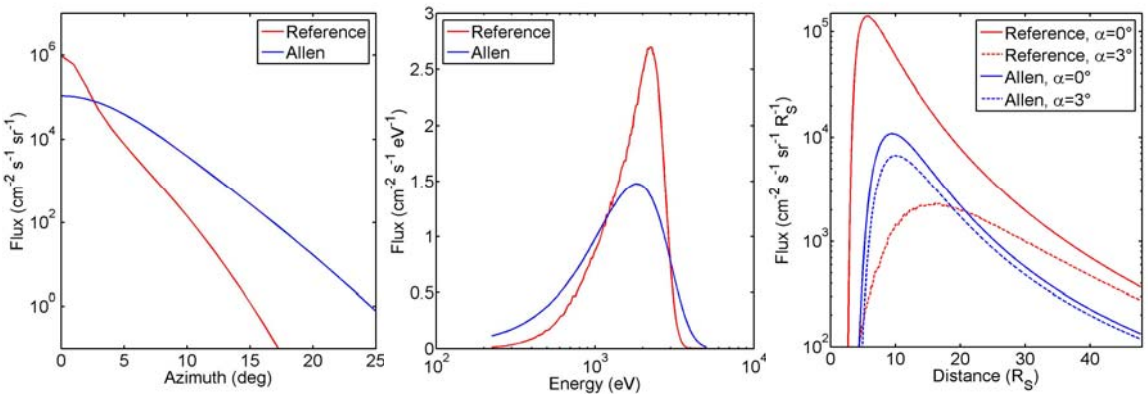

A) **B)** **C)**

Figure 1.2. Differential flux (cm^{-2} s^{-1} sr^{-1}) versus azimuthal direction along the ecliptic plane, with 0 towards the Sun (panel A) and differential flux per unit energy versus energy (panel B) for the two fast solar wind models. Panel C: differential flux (cm^{-2} s^{-1} sr^{-1} R_S^{-1}) versus distance for the fast solar wind reference model and the Allen model for different azimuthal angles indicated in the boxes.

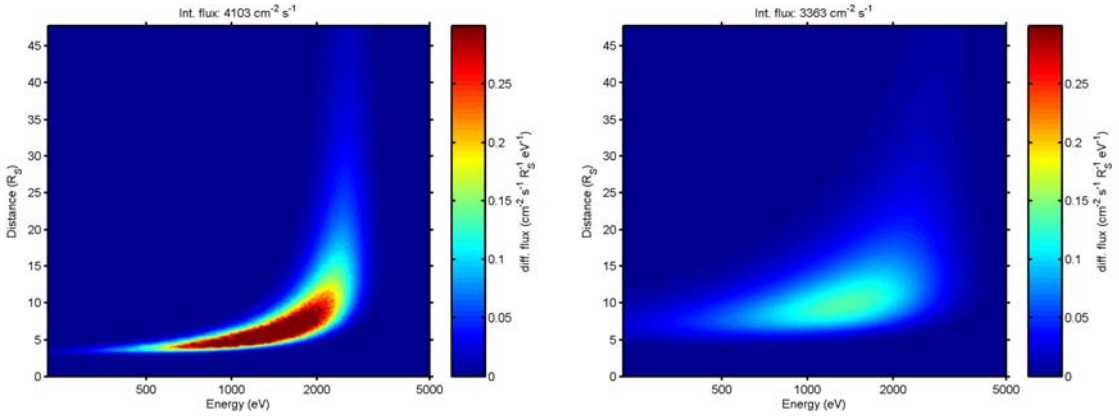

A) **B)**

Figure 1.3. Contour plot of the differential flux per unit distance and energy at 48 R_S as a function of energy and distance for the fast solar wind reference (panel A) and Allen (panel B) models. The flux is integrated over all directions.

due to higher proton temperature close to the Sun in the latter model. Hence, these examples show that the measure of the energy and angular distribution of the neutral solar wind can yield information about the solar wind proton temperature.

Figure 1.2C shows the neutral differential flux, integrated over all energies between 200 eV and 5 keV, as a function of the distance of the generation region for different azimuth directions. Both models, which include loss mechanisms or mean free path for neutrals before being detected, predict that most of the neutral signal (solid line for the central direction) is generated below or around 10 R_S. In fact, for R > 10 R_S, the loss-rate decreases significantly, and most of the neutrals can propagate up to the SolO position. Hence, the detected neutral signal reflects the properties of the solar wind at about 10 R_S. As we scan in azimuth, moving away from the central direction (dashed lines in Figure 1.2C), the flux decreases and the generation region shifts towards higher

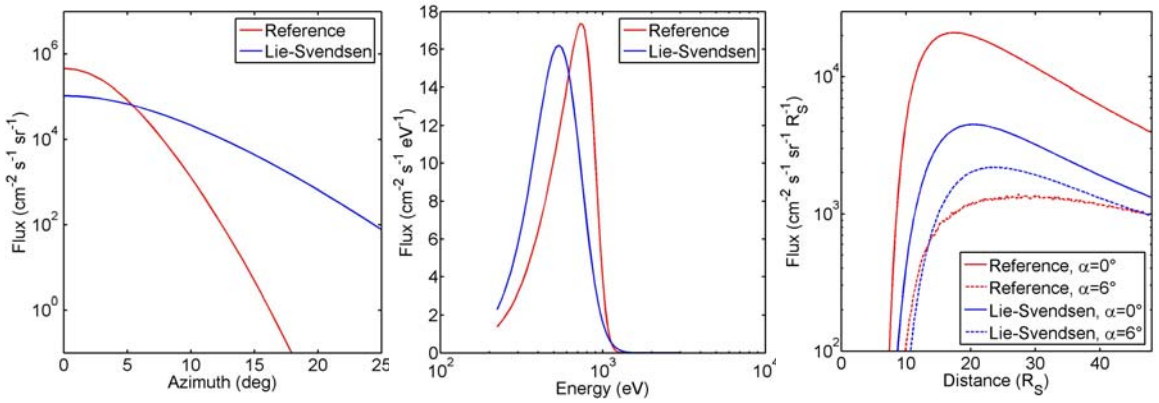

A) **B)** **C)**

Figure 1.4. Differential flux (cm^{-2} s^{-1} sr^{-1}) versus azimuthal direction along the ecliptic plane, with 0° towards the Sun (panel A) and differential flux per unit energy versus energy (panel B) for the two slow solar wind models. Panel C: differential flux (cm^{-2} s^{-1} sr^{-1} R_S^{-1}) versus distance for the slow solar wind reference model and the Lie-Svendsen model for different azimuthal angles indicated in the boxes.

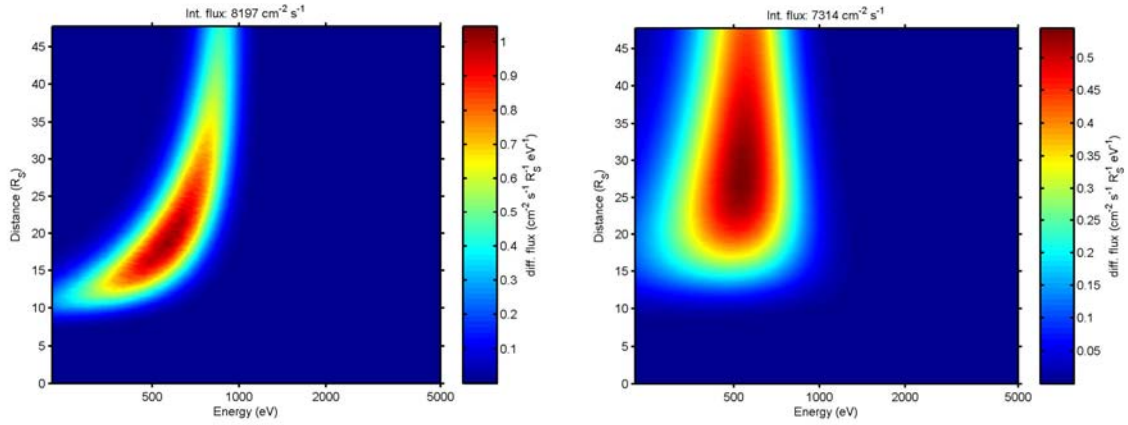

A) **B)**

Figure 1.5. Contour plot of the differential flux per unit distance and energy at 48 R_S as a function of energy and distance for the slow solar wind reference (panel A) and Lie-Svendsen (panel B) models. The flux is integrated over all directions.

distances from the Sun. This implies that the angular resolution of the neutral flux can yield information about the solar wind properties at different distances.

Figure 1.3 shows the differential flux in an energy-*versus*-distance plane. It illustrates that at larger heliocentric distances, most of the neutrals are generated at higher energies in the region where the solar wind is accelerating. The acceleration region seems to be broader for the Allen model (panel B).

1.3.1.2. Models for slow solar wind neutrals

Similar simulations are performed to study the neutral signal from the slow solar wind, by using the "reference" and the "Lie-Svendsen" models. Basically, all considerations

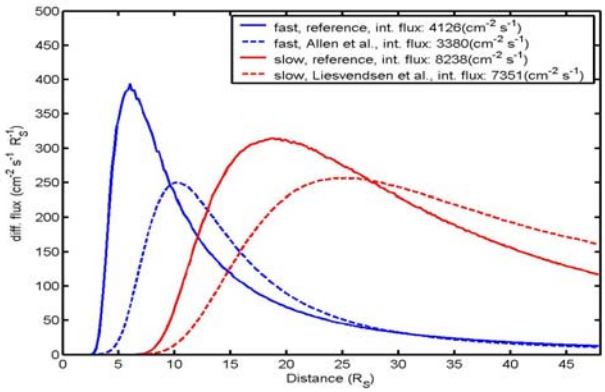

Figure 1.6. ENA differential flux at 48 R_S, as a function of the generation distance, integrated over all energies and directions, for different solar wind conditions and models.

about fast solar wind apply also here; however, the neutral solar wind fluxes are higher (about 8 10^3 cm^{-2} s^{-1}). Also here, the differences between simulated differential fluxes, in angle and energy (Figure 1.4A & B) are mostly due to a different value of the proton temperature in the two models, hence again illustrating the capability for remote-sensing the proton temperature by means of a neutral solar wind measurement.

Figure 1.4C, shows that neutrals in the slow solar wind are generated at larger distances (about 15-20 R_S) in comparison with the fast solar wind. This is mostly due to the fact that the slow neutrals take more time to reach the instrument, and hence they experience more losses for photon and collisional ionization, and charge-exchange.

Figure 1.5 shows the differential flux in an energy-*versus*-distance plane. The considerations for Figure 1.5A (reference model) are similar to those for Figure 1.3A, i.e. most of the neutrals are generated in the region where the solar wind is accelerating. However, Figure 1.5B shows that, for the "Lie-Svendsen" model, the neutrals are generated in a region where the solar wind is "cooled", since the most evident effect is the fact that, as the distance increases, the energy spread of the generated signal decreases.

Figure 1.6, which shows a summary of the ENA flux at 48 R_S, integrated in energy and angle, for all fast and slow solar wind models, makes it clear that these measurements can enable the discrimination between different solar wind models as well as solar wind conditions.

1.3.2. Models of the inner source neutral hydrogen

If the inner source ions originate, as usually assumed, from ionization of neutral atoms released into the solar wind, the neutral hydrogen solar wind is produced at a rate equal to the production rate of the inner source pick-up ions times the probability that the ionization occurs via charge-exchange with the solar wind protons. A flux of inner source pick-up protons of a few tens of t/s as suggested by Ulysses data corresponds to a neutral solar wind contribution of 5 10^4 cm^{-2} s^{-1} at SolO's perihelion. This would swamp the estimated coronal contribution at a few 10^3 cm^{-2} s^{-1}.

Figure 1.7 shows the source function (production rate times the loss factor) for the inner source neutral solar wind hydrogen flux as a function of distance from the Sun for three solar wind models (Allen *et al.*, 2000, and two versions of Lie-Svendsen *et al.*, 2003). The observation point is at 48 R_S with the line of sight pointing sunwards. We assume that the inner source mechanism is as suggested by Schwadron *et al.*, (2000): the solar

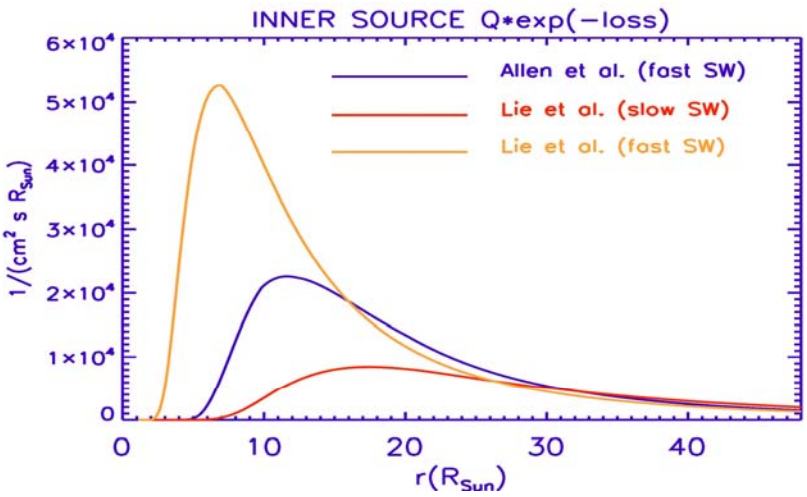

Figure 1.7. Production rate times the loss factor for the inner source neutral hydrogen solar wind along the radial direction between the Sun and the observation point at 48 R_S.

wind ions strike the dust grains and release implanted atoms from previous solar wind impacts. The latter have approximately solar wind abundances, although the hydrogen is suppressed by about a factor of 5 (hydrogen/oxygen ratio = 310). The production rate is proportional to the product of the solar wind flux times the dust geometrical cross section. Note that the dust geometrical cross section needed to produce the observed amount of pick-up ions by this mechanism is at least two orders of magnitude higher than expected from the models of the circumsolar dust cloud. The neutral solar wind flux at 48 R_S is 6.25 10^4 cm^{-2} s^{-1} (slow SW) and 7.5 10^4 cm^{-2} s^{-1} (fast SW). The source function is peaked near the Sun, but not as sharply as the coronal source, so that the information provided would refer to the distances further away from the Sun.

If the neutrals released from the inner source do not come from the recycled solar wind but from the material of dust grains, the fraction of hydrogen, and thus the inner source protons, would be much lower than following from the above mechanism. Assuming that the number of released hydrogen atoms is equal to that of oxygen and carbon (from observations, 2 t/s each), the expected neutral solar wind flux would be of the order of 10^3 cm^{-2} s^{-1}.

The angular spread of the inner source contribution is equal to the proton solar wind angular spread averaged over the source region. For Lie-Svendsen solar wind models this corresponds to the cone of half opening angle 9 deg (fast SW) and 13 deg (slow SW). A summary of the expected distribution features is shown in Table 1.1.

1.3.3 Models for neutral solar wind helium

The helium component of the neutral solar wind results from neutralization of the solar wind alpha particles by double charge exchange with the interstellar helium background. The estimated flux at 0.2 AU is 10^3 cm^{-2} s^{-1}, which is much higher than the neutral helium flux from other sources. The contribution from the solar corona is negligible due to very low neutral helium fraction (10^{-9} as compared to 10^{-6} ~ 10^{-7} for neutral hydrogen). Also, the inner source helium contribution is comparatively

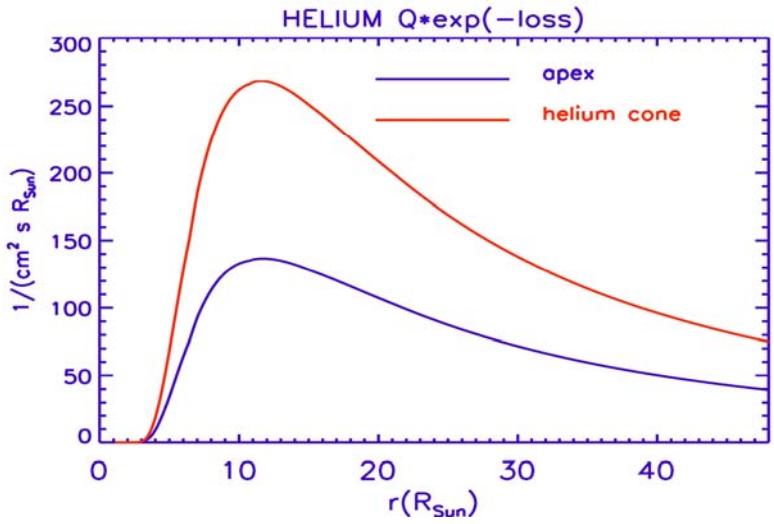

Figure 1.8. The production rate times the loss factor for the neutral solar wind helium along the radial direction between the Sun and the observation point at 48 R_S.

unimportant, because the interstellar helium density near the Sun is enhanced by Sun's gravitation.

Figure 1.8 shows the source function of the neutral helium solar wind calculated using a simple cold model for the interstellar helium distribution and the slow solar wind model from Lie-Svendsen *et al.*, (2003). The fast wind case corresponds to the energy of the helium atoms that would exceed the upper limit of 5 keV for neutral particle instrument. The calculated neutral helium solar wind flux at 48 R_S is 10^3 cm^{-2} s^{-1} in the interstellar medium (ISM) apex direction and 1.9 10^3 cm^{-2} s^{-1} in the region of the interstellar helium cone.

The source of the neutral solar wind helium is characterized by a spatial distribution that is qualitatively different from the sources of the neutral hydrogen solar wind. The coronal neutral solar wind source and the inner source are concentrated near the Sun. The neutral solar wind helium source is a product of the solar wind alpha flux and the interstellar helium background, which varies relatively slowly with distance. As a result, observations of the neutral helium solar wind would provide a different view of the solar wind radial evolution, with the region further away from the Sun contributing the dominant part of the flux.

A potential application could be to estimate (and subtract) the contribution to the neutral hydrogen solar wind coming from the larger heliocentric distances to emphasize the coronal contribution. With an upper energy limit of 5 keV/amu observations of neutral helium solar wind would be effectively restricted to the slow solar wind regions.

1.4 SCENARIO Scientific Objectives

From previous Sections, it follows that the NSW signal should be considered as a fundamental tool for investigating the inner heliospheric plasma features. Hence, the primary Scientific Objectives are formulated on the original SolO objectives listed in

Section 1.1, in terms of SCENARIO's capability of '*remote-sensing'* the Solar Wind in expansion and to study the effect of CMEs on the NSW signal. Other scientific objectives of fundamental importance for the understanding of the heliospheric environment - although not directly linked to SolO primary goals- are listed separately in Section 1.4.3, with reference to the *in situ* characterization of the NSW, as well as to possible other environment-induced effects (like the inner source or the inflowing interstellar gas, see Section 1.2.2). We want to emphasize that a basic contribution to the assessed goals emerges from direct and continuous comparison with the SWA data, and for this reason we strongly suggest to include SCENARIO within that package. In this case, optimizing system resources by DPU sharing can be also realized (see Section 2).

1.4.1 Summary of expected NSW signal intensities

In summary, the observed NSW signal will be originated by means of three basic source configurations, which may consequently determine the NSW signal properties at the vantage point. In Table 1.1, the expected fluxes are listed according to simulations and considerations given in the previous section. To indicate the angular spread of the signal in the different cases, we also give an approximate value of the full-width half maximum of the angular distribution (assuming, for simplicity, a Gaussian distribution). Where possible, both differential fluxes (in angle) and integrated fluxes are listed; in this case, the latter parameter is obtained integrating over all directions. The table is the scientific reference for the "instrument requirement table" (Table 1.2).

Table 1.1

NSW signal origin		**Expected flux (SolO perihelion)**		**Expected flux (SolO aphelion)(2)**		**Angular spread**
Intrinsic neutral solar wind (Section 1.2.1)	Slow SW	10^4 cm^{-2} s^{-1} (integrated[1])	5 10^5 cm^{-2} s^{-1} sr^{-1} (peak)	10^3 cm^{-2} s^{-1} (integrated)	$5{\cdot}10^4$ cm^{-2} s^{-1} sr^{-1} (peak)	10°×10°
	Fast SW	$3{\cdot}10^3$ cm^{-2} s^{-1} (integrated[1])	10^6 cm^{-2} s^{-1} sr^{-1} (peak)	3 10^2 cm^{-2} s^{-1} (integrated)	10^5 cm^{-2} s^{-1} sr^{-1} (peak)	5°×5°
Neutral solar wind from charge exchange with the gas in the heliosphere (Section 1.2.2)	Slow SW	10^3 cm^{-2}s^{-1} ÷ 10^5 cm^{-2}s^{-1}		10^2 cm^{-2}s^{-1} ÷ 10^4 cm^{-2}s^{-1}		13°×13°
	Fast SW	10^3 cm^{-2}s^{-1} ÷ 10^5 cm^{-2}s^{-1}		10^2 cm^{-2}s^{-1} ÷ 10^4 cm^{-2}s^{-1}		9°×9°
ENAs from seed particles for SEP in CME (Section 1.2.3)		10^3 cm^{-2}s^{-1} ÷10^6 cm^{-2}s^{-1}		10^2 cm^{-2}s^{-1} ÷10^5 cm^{-2}s^{-1}		5°×5°

(1) The differential flux is integrated over the solid angle indicated in the last column.
(2) Fluxes at aphelion are scaled by $(R_p/R_a)^2 = 1/10$

1.4.2 Primary Scientific Objectives

All the objectives listed here below (extracted from SolO Payload Definition Document) will be addressed by SCENARIO, and are linked to speculations and studies described in Sections 1.2 and 1.3.

1.4.2.1 Objectives related to SolO PDD point: "Determine the properties, dynamics and interactions of plasma, fields and particles in the near-Sun heliosphere"

- **Radial evolution of solar wind structures in the inner heliosphere**

The Solar Wind Analyzer (SWA) *in situ* measurements will allow estimates of SW evolution from a single vantage point. Hence, only mixed temporal evolution will be monitored (or a mixture of temporal and spatial evolution during the non corotational phase), at a given distance from the Sun, with the goal to '*... provide observational constraints on kinetic plasma properties for a fundamental and detailed theoretical treatment of all aspects of coronal heating*'. A crucial and fruitful complement to such measurements would come from SCENARIO SW remote sensing capability, which will give a concrete chance to expand our knowledge about SW evolution (flux intensity, energy and temperature) by means of multi-point analysis along the SW expansion path.

- **Influence of CMEs on the structure of the inner heliosphere**

Continuous measurements of the NSW will open a possibility to directly study the dynamics of major transient processes in otherwise inaccessible regions of propagating coronal mass ejections (CMEs). Indeed, SCENARIO will be able to observe a critical part of the energy distribution that will determine whether suprathermal tails exist in the distribution close to the Sun (15÷20 R_S) during quiet times, or just during CME events.

- **Solar wind microstate evolution with radial distance**

The capability of SCENARIO to detect atoms neutralized below 20 R_S represents a unique possibility to access to information about the kinetic state of the plasma below the Alfvén radius. This distance is also crucial for discriminating the Alfvénic turbulence propagating modes, since MHD turbulence is completely different moving across this radius.

1.4.2.2 Objectives related to SolO PDD point: "Investigate the links between the solar surface, corona and inner heliosphere".

- **Acceleration and heating mechanisms that lead to coronal hole –associated fast solar wind**

Remote sensing via SCENARIO measurements will allow determination of fast solar wind spatial evolution along its path inside the inner heliosphere. Thus, parallel temperature profiles versus radial distance, when compared to both SWA *in situ* measurements and coronograph data (which will be effective in perpendicular temperature estimates, see D'Amicis et al., 2007), will provide useful information on both fast streams acceleration and heating mechanisms.

- **Sources of slow solar wind, and what is its temporal and spatial evolution**

Similarly to fast SW, also slow solar wind remote sensing via SCENARIO measurements would allow determination of dynamics along its path inside the inner heliosphere. Hence, if SWA measurement will provide information about the location of

slow solar wind sources, SCENARIO will consistently support investigations about its spatial evolution.

- **Sources and the global dynamics of eruptive events (CMEs) and what are their effects on the inner heliosphere**

This objective may be studied by combining remote sensing the early stage of CME in UV by the coronograph on SolO and optical observations on Earth, and *in situ* measurement of energetic particles accelerated by the CME-driven shock by SWA and particle detectors located on Solar Orbiter as well as Solar Sentinels. To reach a fuller understanding of this propagating and expanding phenomenon, however, SCENARIO data will be crucial, because only direct sampling of the CME-associated ion population via ENA can we discern the evolution of the shock before it passes by the *in situ* particle detectors.

1.4.2.3 Objectives related to SolO PDD point: "Explore, at all latitudes, the energetics, dynamics and fine-scale structure of the Sun's magnetized atmosphere"

- **Nature of coronal hole boundaries, how do they evolve and how do they project into the inner heliosphere**

SW shock boundaries are usually monitored by *in situ* plasma measurements, taking advantage of spacecraft motion and/or temporal variations, but nevertheless only one point in space. SCENARIO, on the other hand, by measuring plasma at a distance via ENA, will permit a third kind of investigation. In fact, the angular resolution of the neutral flux can yield information about the solar wind properties at different distances. Hence, thanks to the NSWD angular scanning, possible locations of SW regimes upstream as well as downstream the shock boundary will be monitored at the same time.

1.4.3 Other Scientific Objectives

- ***In situ* characterization of the Solar Wind**

Other than the usual charged components (always firmly addressed in most of past investigations), the actual solar wind does include a neutral component, never observed before. SCENARIO will clearly measure such a component, defining its relative contribution with respect to the other ionized components. As an independent scientific goal, we want to assess these intrinsic characteristics in the frame of *in situ* measurements. This characterization will complement the ionized SW remote sensing capabilities of the NSW signal and will take advantage from simultaneous SWA measurements.

- **Distribution and intensity of the inner source**

Energetic neutral atoms can also come from solar-wind protons and alpha particles after charge exchange with slow-moving neutral atoms and particles in the inner heliosphere, which do not belong to the solar wind. Although the presence and distribution of this signal is still unclear, simulations show that the inner source-originated NSW exhibits

basically similar properties to the intrinsic NSW and provides a similar remote sensing capability. Anyway, the NSW intensity is much higher if such an interaction occurs, so that a full characterization of intensity and distribution of the inner source particles could be accomplished.

- **ENA radiation from other heliospheric sources**

Besides the inner heliosphere, the outer heliosphere is also a well-known source for energetic neutral atoms, i.e. energetic ions which transcharged with the local interstellar medium in remote regions far from the Sun, which travel on ballistic trajectories unaffected by the interplanetary magnetic fields into the inner heliosphere region. Observation of fluxes will allow to study the interaction or even "ping-pong" passages of the particles due to the ensuing ionising and neutralisation processes of the heliospheric energetic ion and neutral populations of the outer and inner heliosphere, and add to the data sets of the forthcoming IBEX and SENTINEL missions.

1.4.4 Summary

Table 1.2 shows a summary of the scientific performance requirements related to the scientific objectives listed in the previous sections.

Table 1.2: Scientific performance requirements

Scientific Objective	Expected flux[(1)] (cm^{-2} s^{-1})	Energy range[(2)] (keV)	Energy resolution[(3)] (dE/E)	Angular spread[(4)] (°)	Angular resolution[(5)] (°)	Time resolution[(6)] (m)
Radial evolution of solar wind structures in the inner heliosphere	$10^3 \div 10^4$	0.5 ÷ 2	25 %	~10×10	~2	≤60
Influence of CMEs on the structure of the inner heliosphere	$10^3 \div 10^6$	1÷5	25 %	~5×5	~1	≤10
Solar wind microstate evolution with radial distance	10^3	0.5 ÷ 2	25 %	~10×10	~2	≤60
Acceleration and heating mechanisms that lead to coronal hole –associated fast solar wind	10^3	1 ÷ 5	25 %	~5×5	~1	≤60
Sources of slow solar wind, and what is its temporal and spatial evolution	10^4	0.5 ÷ 2	25 %	~10×10	~2	≤60
Sources and the global dynamics of eruptive events (CMEs) and what are their effects on the inner heliosphere	$10^3 \div 10^6$	2 ÷ 5	25 %	~5×5	~1	≤60

Nature of coronal hole boundaries, how do they evolve and how do they project into the inner heliosphere	10^3	0.5 ÷ 2	25 %	~5×5	~1	≤60
***In situ* characterization of the Solar Wind**	10^4	0.5 ÷ 5	25 %	N/A	N/A	≤60
Distribution and intensity of the inner source	10^4	0.5 ÷ 2	25 %	~10×10	~2	≤60
ENA radiation from other heliospheric sources	N/A	0.5 ÷ 5	25 %	N/A	N/A	N/A

(1) Flux that we need to measure to reach the scientific objective (rough estimation); (2) energy range we need to cover; (3) needed energy resolution; (4) angular field of view we need to cover; (5) needed angular resolution; (6) needed time resolution.

Appendix 1: Simulations details

Here we describe the SW "reference" model used to simulate ENA flux. In all cases, it is assumed that the proton density, n_p= 0.83 n_e, where n_e is the electron density. For the fast solar, the electron density is taken from Guhathakurta *et al.* (1999). The electron temperature from David *et al.* (1998) at low heliocentric distances is extrapolated to reach 10^5 K at 1AU (Schwenn, 1990). For the proton temperature, T_p, data are taken from Helios for 0.3 to 1 AU (Marsch, 1991) and extrapolated to 1 R_S with a boundary value of 10^6 K at 1 R_S. The outflow velocity is taken from a semi-empirical model compatible with inferences from the UltraViolet Coronograph Spectrometer (UVCS) at low heliocentric distances with an asymptotic outflow velocity of 700 km/s. For the slow solar wind, the density is taken from Antonucci *et al* (2005) for the corona and extrapolated to reach an asymptotic value of 10 cm^{-3} at 1 AU. The electron temperature is taken from Gibson *et al.* (1999) up to 5 R_s, and extrapolated beyond using the Helios radial trend (Marsch, 1991). The proton temperature is derived like for the fast wind except that T_p = 2 10^6 K at 1 R_S. The hydrogen

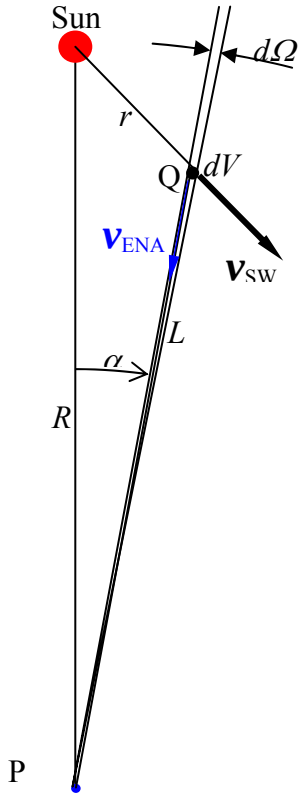

Figure A1. Geometry for simulations. The ENA flux of velocity v_{ENA} arriving at P from the given azimuth α is integrated along the line of sight from P to infinity. The volume element dV for integration at Q is at distance r from the Sun, L from P; and $d\Omega$ is the solid-angle element subtended by dV at P. The solar-wind velocity at Q (v_{SW}) is radial. The solar-wind temperature provides v_{ENA} along the line of sight. Sun is at (0, 0, 0); NSWD is at P (0, -48 R_S, 0) (the figure is not to scale).

outflow velocity is taken from Sheeley *et al.* (1997).

In the reference frame for the calculations (see Figure A1), the Sun is at (0,0,0), the NSWD is at ***P*** (0,-48,0), and the generic ENA infinitesimal source is at ***Q***, at a distance ***r*** from the Sun**.** The reference frame is at rest, and aberration effect due to the S/C velocity is not considered (see Section 3 for a detailed discussion of this effect). The ENA flux at ***P*** is then calculated by integrating along the *line of sight* ***L***; α is the azimuth angle from Sun's direction. The flux generated in the volume ***dV*** placed at the point ***Q*** is due to radiative recombination ("*rec*") and charge-exchange (Hasted, 1964). The plasma inside ***dV*** is assumed to have a maxwellian distribution *f(E, v)*. The rate of neutral particles generated inside ***dV*** is:

$$r = n_p \left(\frac{1}{\tau_{ce}} + \frac{1}{\tau_{rec}} \right) dV \, .$$

The charge-exchange frequency can be calculated (assuming that the thermal velocity is a mean value for the relative velocity between ions and neutrals) as:

$$\frac{1}{\tau_{ce}} = n_H \, \sigma_{ce} \, v_{th} \, .$$

The rate for radiative recombination is

$$\nu_{rec}(r) = 2.1 \cdot 10^{-11} n_e(r) T_e(r)^{-1/2} \Phi(T_e) \, ,$$

where $\Phi(T_e)$ is a weak function of electron temperature (Spitzer, 1962). Then we integrate from ***P*** along ***L*** to obtain the total flux (line of sight integration):

$$\frac{dJ}{dE \, d\Omega} = \int_0^\infty n_p \left(\frac{1}{\tau_{ce}} + \frac{1}{\tau_{rec}} \right) f\left(E, \hat{v}\right) dL \, .$$

Once a neutral is generated at ***Q,*** it may be ionized again before reaching ***P*** due to photoionization ("*v*"), collisional ionization ("*c*") or charge-exchange (this process is both source and loss of neutrals). Such processes are included in the model by multiplying each infinitesimal flux by the probability *p* for an ENA to go from the generic point ***Q*** to ***P*** (D'Amicis *et al.,* 2007):

$$p = \exp\left(- \int_0^L \left(\frac{1}{\lambda_{ce}} + \frac{1}{\lambda_v} + \frac{1}{\lambda_c} \right) dL \right) .$$

The loss rate for photoionization (Olsen et la, 1994) is:

$$\nu_v(r) = 4 \cdot 10^{-3} (R_S / r)^2 \, ,$$

while the loss rate for collisional ionization by electrons is:

$$\nu_c(r) = 6.2\times10^{-11} n_e(r) T_e^{1/2}(r) \exp(-\chi / kT_e(r)) .$$

References

Aellig M.R., *et al*., *Geophys. Res. Lett.*, 28, 2767 (2001)
Allegrini, F., *et al.*, *J. Geophys. Res*., 110, A05105 (2005)
Allen, L.A., *et al.*, *J. Geophys. Res*., 103, 6551 (1998)
Allen, L.A., *et al.*, *J. Geophys. Res*., 105, 23123 (2000)
Antonucci, E., *et al.*, *Astron. & Astrophys.*, 435, 699-711 (2005).
Barabash, S., *et al*., *Planet. Space Sci.*, 55, 1772 (2007)
Bochsler, P., *et al*., *Geophys. Res. Lett.*, 33, L06102 (2006)
Brinkfeldt, K., *et al*., *Icarus*, 182 (2) 439 (2006)
Bruno, R., and Carbone, V., *Living Reviews in Solar Physics*, 2, 4 (2005)
Cohen, C., *et al.*, *J. Geophys. Res*., 106, 20979 (2001)
Collier, M. R., *et al.*, *Adv. Space Res*., 34, 166 (2004)
D'Amicis, R., *et al.*, *J. Geophys. Res.*, 112(A11), 6110 (2007)
David, C., *et al.*, *Astron. Astrophys*., 336, L90-L94 (1998)
Fahr, H., *et al.*, *Rev. Geophysics*, 45, RG4003 (2007)
Gabriel, A. H., *et al*., *Astrophys. J.*, 169, 505 (1971)
Geiss, J., *et al.*, *J. Geophys. Res*., 100, 23373 (1995)
Gibson *et al*., *J. Geophys. Res.*, 104, 9691-9700 (1999)
Gloeckler, G., and Geiss, J., *Sp. Sci. Rev*., 86, 127 (1998)
Gruntman, M., *J. Geophys. Res*., 99, A10, 19213 (1994)
Gruntman, M., *Rev. Sci. Instr*., 68 (10), 3617 (1997)
Gruntman, M., and Izmodenov, V., *J. Geophys. Res*., 109, A12108 (2004)
Guhathakurta, M., *et al.*, *J. Geophys. Res.,* 104(A5), 9801-9808 (1999)
Hasted, G. B., Physics of Atomic Collisions, 416 pp., Butterworths, London, (1964)
Hilchenbach, M., *et al*., *Astrophys. J.*, 503, 916, (1998)
Hsieh, K. C., *et al.*, *Astrophys. J.*, 393, 756 (1992)
Kahler, S. W., *et al.*, *Astrophys. J.*, 562, 558 (2001)
Kahler, S.W., *et al.*, *Astropys. J.*, 290, 742 (1985)
Kahler, S. W., *et al.*, *Sol. Phys*., 107, 385 (1987)
Kohl, J. L., *et al.*, *Sol. Phys.*, 162, 313 (1995)
Kuhn. J. *et al.*, *Astrophys. J.*, 667, L203 (2007)
Lie-Svendsen, *et al.*, *Astrophys. J.*, 596, 621 (2003)
Mann, I., and Czechowski, A., *Astrophys. J*., 621, L73 (2005)
Marsch, E., Physics of the inner heliosphere, vol. 21, 45-133. (1991)
Marsch, E., and Richter, A.K., *Journ. Geophys. Res*., 89, 5386-5394, (1984)
Mason, G. *et al.*, *Astrophys. J.* 535, L133 (1999)
Michels, J. G. *et al.*, *Astrophys. J.* 568, 385 (2002)
Mitchell, D. G. *et al*., *Geophys. Res. Lett.* 28 (6), 1151 (2001)
Möbius, E., *et al.*, *Astr. & Astrophys.*, 426, 897 (2004)
Möbius, E., *et al.*, in *The Solar System*, *Heliosphere*, *and the Galactic Environment of the Sun*, edt. P. Frisch, Springer, 209–258 (2006)
Nitta, N.V., *et al.*, *Astrophys. J.*, 650, 438-450 (2006)
Olsen, E. L., *et al.*, *Astrophys. J.*, 420, 913 (1994)
Orsini, S. *et al*., submitted to *Advances in Geosciences* (2008)
Pizzo, V., *et al.*, *Astrophys. J.*,, 271, 335 (1983)
Reames, D. V., *et al.*, *Astrophys. J.*, 327, 998 (1988)
Reames, D. V., *et al.*, *Sp. Sci. Rev*., 90, 413 (1999)
Schwadron, N.A., *et al.*, *J. Geophys. Res*., 105, 7465 (2000)

Schwenn, R., Physics of the Inner Heliosphere, vol. 20, 99-181, ed. R. Schwenn and E. Marsch (1990)
Sheeley, N.R., *et al.*, *Astrophys. J.*, 484, 472-478 (1997)
Spitzer, L., Physics of fully ionized gases, (ed. Interscience Publishers, New York) (1962)
Wimmer-Schweingruber, R.F., and Bochsler, P., *Geophys. Res. Lett*., 30(2), 1077 (2003)
Withbroe, G. L., *et al.*, *Sp. Sci. Rev.*, 33, 17 (1982)
Wurz, P., in The Outer Heliosphere: Beyond the Planets, (eds. K. Scherer, H. Fichtner, and E. Marsch), 251–288 (2000)
Yashiro, S., *et al.*, in ASP Conf. Ser. 325, The Solar-B Mission and the Forefront of Solar Physics, ed. T. Sakurai, & T. Sekii (San Francisco: ASP), 401 (2004)

2 TECHNICAL DESCRIPTIONS AND DESIGN

2.1 Introduction

The current design of the Neutral Solar Wind Detector, SCENARIO, proposed for SolO has been derived from very fruitful discussions within the NSWD team, tests and simulations to overcome several constraints, especially the minuscule signal-to-noise ratio ($< 10^{-6}$) confronting any attempt to measure the neutral component of the solar wind (NSW). With an expected minimum ENA flux of 10^3 cm^{-2} s^{-1} within a *Field Of View* (FOV) of the order of 5°÷10° (both in elevation and azimuth), based on realistic simulations (see Tables 1.1 and 1.2), the driving design parameter has been the integrated geometrical factor, which needs to be $>10^{-3}$ cm^2 (see Table 2.1). This has imposed several limitations on the anti-coincidences techniques impacting on the geometrical aperture and the overall efficiency. In addition, being classified as an augmentation payload, optimally light and simplified architecture is required to minimize the demand on the S/C resources such as mass, power and viewing configuration. The following section describes SCENARIO, as designed to meet these constraints. In section 3 we will describe the SCENARIO scientific performances according to science simulations and instrument description.

2.2 Instrument Design Elements including their design maturity

Detecting and characterizing neutral atoms in the energy range of interest, 0.1 ÷ 5.0 keV, in an environment of intense photon, electron and ion fluxes, require 1) highly effective suppression of photons, electrons, ions and 2) a means to ascertain that the particle detected is indeed a neutral atom of the known energy. Before we describe in details the SCENARIO instrument, we note that our unique approach is made possible by a piezo-driven, high-frequency shuttering, multiple nano-slit system, which has its heritage traced to the instrument SERENA on ESA BepiColombo mission to Mercury. The shuttering slits provide, in addition to photon suppression, a precise START signal mark for the time-of-flight (TOF) measurement for each incident energetic neutral atom (ENA). The technique of neutral-ion conversion surface has its heritage traced to LENA on NASA's IMAGE. The electrostatic analyzer (ESA) can be switched on and off at fast frequency, to provide a second time coincidence. The MCP STOP signal will be used with these two correlated signals to complete a triple-coincidence TOF measurement. The technique of conversion surface has its heritage traced to LENA on NASA's IMAGE. This triple-coincident TOF system, located behind a series of charged-particle suppressing electrostatic lenses, provides a sliding 1°×5° IFOV (Intrinsic FOV) scanning out of 12°×5° FOV in order to explore with high angular accuracy the neutral distribution along the aberration direction, defined by the S/C motion.

All the NSWD operations are managed by an FPGA based microcontroller (Sensor Control Unit - SCU). It controls the switching of the power to the individual subsystem (e.g. HV blocks), samples the data, and provides internal intermediate storage and data transfer to the external S/C SpaceWire interface or an external hosting DPU, like the DPU of the SWA package. NSWD will benefit of the inheritance from the SERENA BepiColombo design of the system control and power distribution unit.

The NSWD sensor consists of the following subsystems (see Figure 2.1):
A) Cover (not shown); **B)** Lens group #1: –5kV lens; **C)** Lens group #2: +5kV lens; **D)** Parallel plate collimator, balanced biased +5kV –5kV; **E)** Shuttering system; **F)** Lens group #3: +5kV lens; **G)** Conversion Surface; **H)** Parallel grids ESA: +3kV; **I)** MCP detector; **J)** 2D Anode system (not shown).
The cover protects the instrument when not in operation. The ion/electron suppression

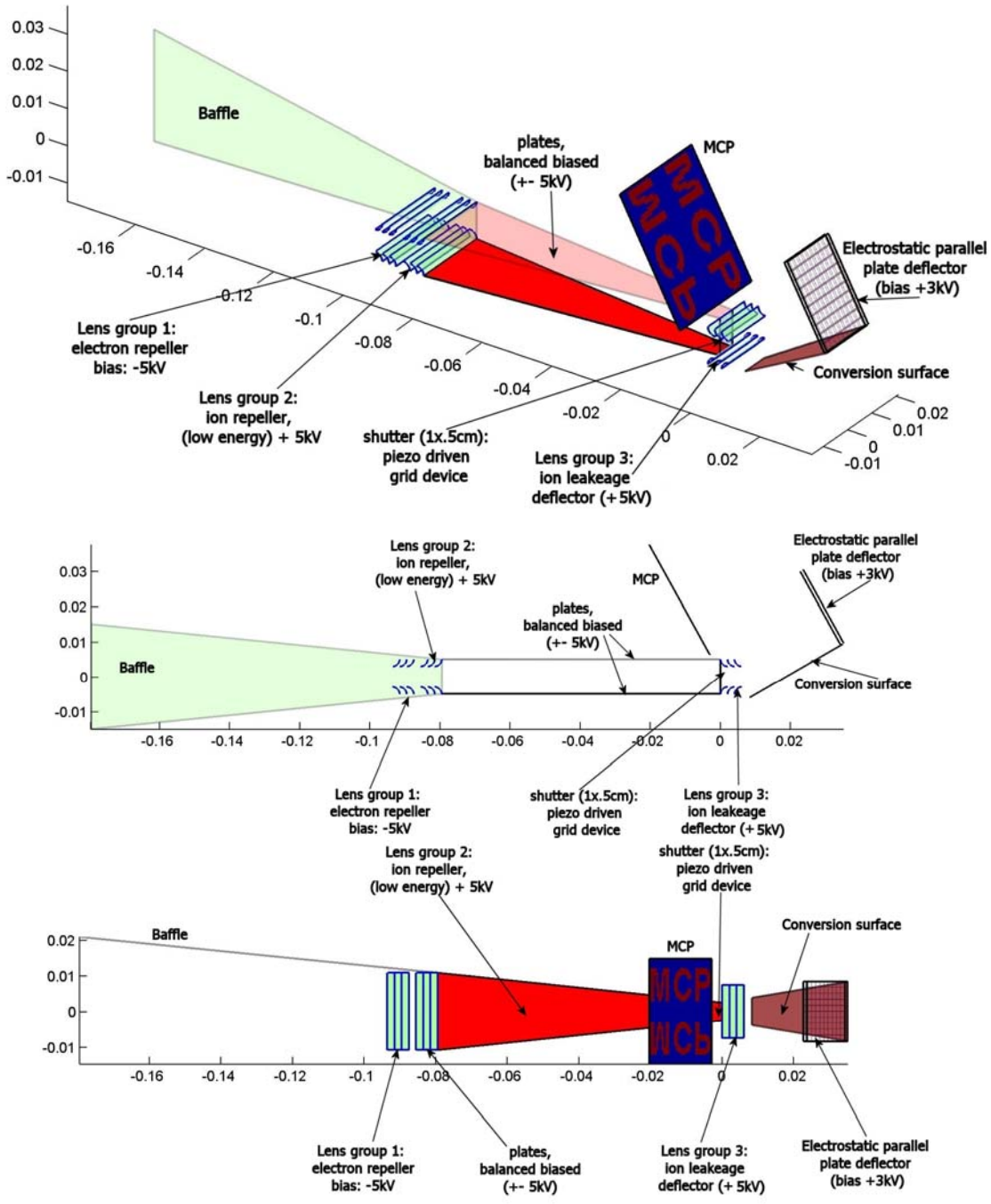

Figure 2.1. SCENARIO elements. From top: 3D view, lateral view, top view.

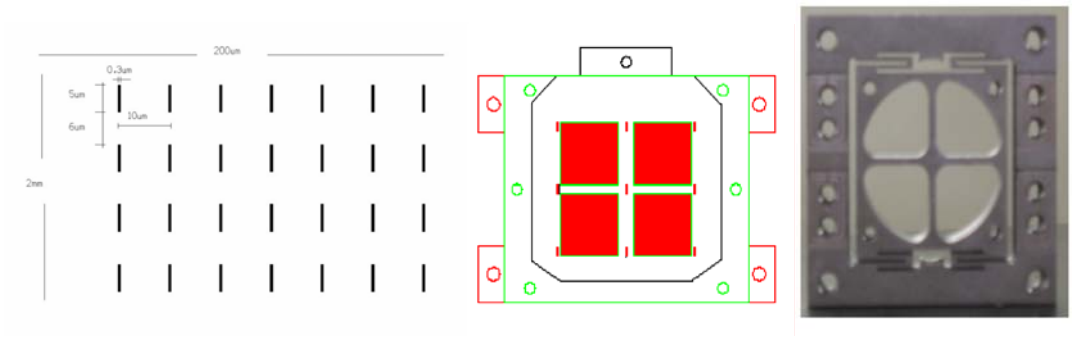

(A) **(B)** **(C)**

Figure 2.2. (A): Schematic view of the geometry proposed for the grids of the shuttering element of SCENARIO. See also Figure 2.3. (b): the whole SCENARIO shuttering element is made of 2 × 2 matrix. Each red area is filled by the grid in (a). (C): The actual ISC ultrasonic oscillator frame sample of ELENA.

system consists of three groups of non-obstructing lens and a parallel plate collimator. Lens group #1 is at –5kV and shall suppress the incoming low-energy SW electrons. Lens group #2 is at +5kV potential; this lens group suppresses the incoming low-energy SW ions. The parallel plate collimator (balanced biased +5kV –5kV), further suppresses the ion/electron distributions of higher energy, not filtered by lens groups #1 and #2, thus limiting the ion/electron leakage impacting onto the following shuttering element.
The shuttering system consists of two identical sheets of nano-slits (see Figures 2.2 and 2.3). While one sheet remains stationary, the other, driven by a piezo oscillator, shuttles back and forth along the width of the slits. Grid openings are of the order of 100 nm or less to act as a filter for Lyman-alpha and other solar radiation. If the oscillator is put in high frequency mode, the alignment of the slits (with a typical duration of tens-hundreds of ns) marks and allows incidence of particles for TOF measurement. The lower limit on the TOF eliminates any photon-initiated signals in the MCP. The upper limit on the TOF sets the threshold of the ENA energy window. The slit dimension and the distance from the front aperture define the 1° × 5° IFOV. A system of piezo-electric actuators controls the relative rest position and distance of the grids. The relative alignment of the two grids can be also used to collimate the ENA flux with a 1°×5° resolution. Hence, the oscillator can be used at very low frequency to make an angular scan through the nominal FOV of 12°×5°.
In summary, the system allows, with respect to the neutral signal:

- to operate a slow sliding 1°×5° scanning within a 12°×5° FOV;
- optionally, to operate a fast (250 ns) shuttering along a 1°×5° specific direction;

and with respect to the UV environment:

- to blind the active detection system when operating in TOF mode;
- to filter Lyman-alpha and other solar radiation when operating in sliding mode.

As a further ion suppression element, we include a lens group #3 (+5kV). This non-obstructing lens suppresses ions originated on or close to the shuttering system and introduces a further defocusing element of the high-energy ion/electron leakage.

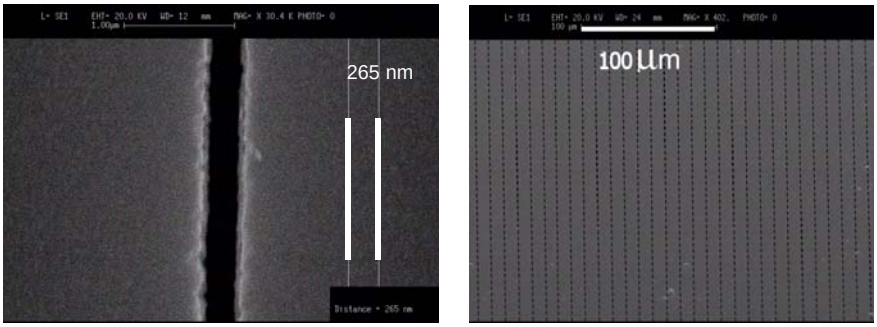

Figure 2.3. (Left) Example of manufactured grid sample (fourth generation) developed for the grids of the NPA shuttering elements of the SERENA/ELENA spectrometer on board ESA/JAXA mission BepiColombo. (Right) Example of full view geometry.

After this group of lenses, only energetic neutral atoms are able to reach the conversion surface, which converts an impacting ENA to an ion and an electron, with efficiency of the order of 5%.
The emitted electrons are removed thanks to a +100V collector plate, not obstructing any particle path. The ions are emitted at approximately mirroring angles and enter in the parallel grids ESA. The ESA is a high transmittivity electrostatic analyzer, which can be operated in three basic modes:

- fixed biasing, providing the neutral energy dispersion within a range of 100 eV ÷ 5 keV focusing the output beam on the MCP target without the need of stepping energy; all ions are deflected.
- on/off mode, to provide neutral energy dispersion combined with a TOF start information; ions are deflected depending on what time they enter the analyzer.
- stepping voltage, acting as a "low pass energy filter", to provide the integral energy distribution function; ions are deflected depending on their energy.

In all cases, deflected ions fly towards the MCP detector, which releases an electron pulse onto a multi-anode discrete system mapping the hit position on a 2D array. The MCP provides the STOP timing when ESA is operated in ON/OFF mode. The 2D Anode system utilizes a low-noise, low-power multi-channel front-end integrated circuits (ASICs), which process in parallel the multi-anode position detection system. Upon signal detection above the adjustable threshold, the circuits respond with sending out the energy- and position-information of the hit channel. Up to 128 channels for

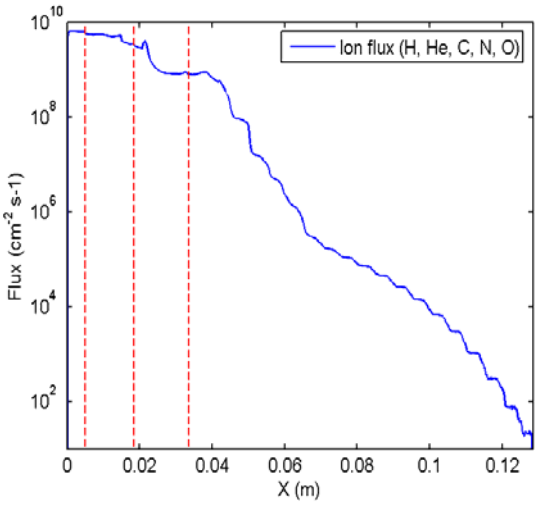

Figure 2.4. Simulation of the ion flux inside the parallel plate high voltage ion deflector. Red dashed lines (from the left): entrance of lens group #1 (electron suppression); entrance of lens group # 2; entrance of parallel plate deflector (at ±5kV).

each chip are accommodated in a single device, thus providing more than 10×10 mapping. Figure 2.4 shows a simulation of the reduction of the SW ion flux (including heavy ions) inside the parallel plate ion deflector. Figures 2.5 and 2.6 show the SCENARIO box.

2.3 Expected Geometrical Factor

Taking into account the instrument elements described in Section 2.2, we estimate an overall geometrical factor of the order of 2 10^{-3} cm^2 (see Table 2.1). Since the flux is highly collimated (and generally expressed in cm^{-2} s^{-1}, see Table 1.2), this number can be used as a reference to be directly multiplied times the fluxes to obtain count rates. If we include the FOV angle, the value is 4 10^{-5} cm^2 sr.

Table 2.1. Geometrical factor of SCENARIO

Element	Value	Unit
Aperture - active grid extent	0.5	cm^2
Geometrical aperture ratio	0.20	
Conversion surface efficiency	0.05	
ESA	0.80	
MCP Efficiency to ion	0.50	
FOV (12°×5°)	0.02	sr
Total, including angle	4 10^{-5}	cm^2 sr
TOTAL	**$2 \cdot 10^{-3}$**	**cm^2**

2.4 Maturity of the design

SCENARIO is an innovative sensor, based on heritage and space-borne components got from CLUSTER/CIS, MARS EXPRESS/ASPERA-3, Venus EXPRESS/ASPERA-4,

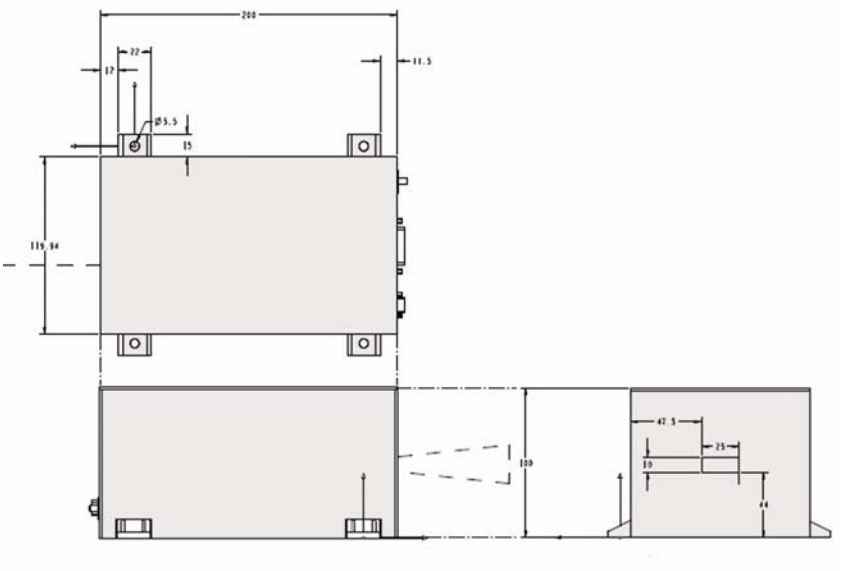

Figure 2.5. SCENARIO box. Dashed lines: baffle.

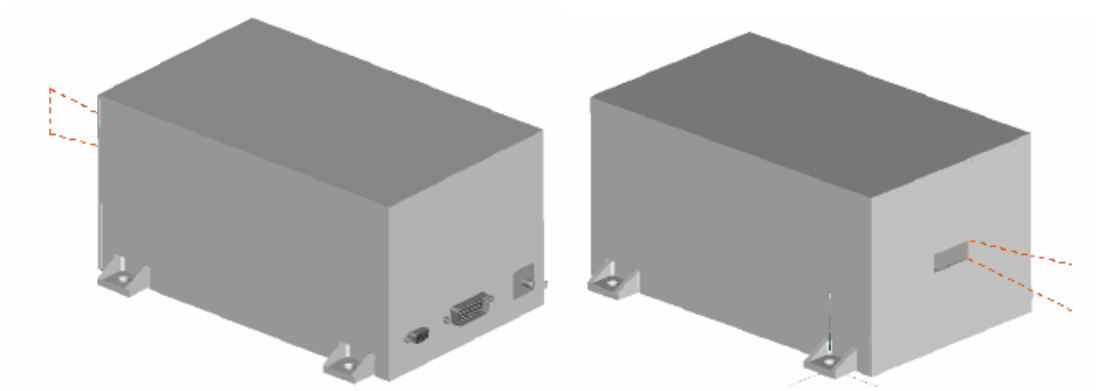

Figure 2.6. SCENARIO box (3D view). The baffle is not drawn (but indicated by dashed lines).

and IMAGE/MENA. At present, these concepts are the basic heritage for the development of the SERENA/ELENA sensor, instrument selected for the BepiColombo project. The sensor maturity is medium, since design and preliminary testing activity are already in advanced process phase.
The thermal criticality is low, all exposed components like collimators and UV grading systems are thermally tested (see IMAGE/MENA), and can support local thermal excursions.

2.5 Accommodation

NSDW should be S/C face pointing towards the Sun, with an offset angle of 15°. An alternative, possible accommodation would be the +Y panel, in a position behind the sunshield and with an unobstructed field of view of ± 6°, 15° off the S/C - Sun axis in the Sun-Satellite plane and about ± 5° out of the plane.

3 INSTRUMENT PERFORMANCE

3.1 SCENARIO Characteristics

Table 3.1 SCENARIO characteristics

Parameter	Value
Energy range	0.1÷ 5 keV
Energy resolution $\Delta E/E$	25%
FOV - Viewing angle	$12^o \times 5^o$
IFOV (Intrinsic FOV) - Angular resolution	$1^o \times 5^o$
Optimal temporal resolution	1 ÷ 60 min
Geometric factor (including angle) $G^* = S\Omega\varepsilon$	$5 \cdot 10^{-5}$ cm^2 sr
Geometric factor $G = S\varepsilon$	$2 \cdot 10^{-3}$ cm^2

3.2 ENA measurement concepts

According to the Scientific Requirement Table 1.2, SCENARIO should detect ENA with fluxes down to ~10^3 cm^{-2} s^{-1}, concentrated in a FOV up to 10°×10°, within the 0.5 ÷ 5 keV range, with an energy resolution (dE/E) of the order of 25% and with a very good angular resolution (~1°×5°). To satisfy all these requirements, we propose the instrument described in Section 2. In fact:

- The energy range of the instrument (0.1 ÷ 5 keV) is more extended than the requested scientific range (0.5 ÷ 5 keV) with the needed energy resolution;
- The FOV of the instrument (12°×5°) covers most of the angular spread of the signal, with the needed angular resolution (1°) in one direction (azimuth):

In this section we discuss the performance (energy and angular resolution) of the instrument. The trajectory of a neutral energetic atom inside the instrument is shown in Figure 3.1.

The angular resolution can be obtained in two modes: 1) by analyzing the azimuth position of the stop signal on the MCP (in the azimuth direction, i.e. out of the plane of

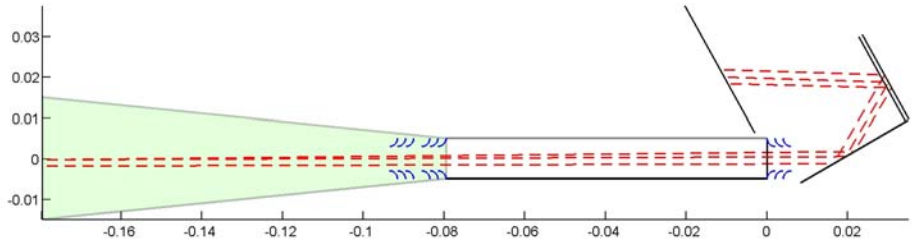

Figure 3.1. Examples of particle trajectories (red dashed lines) inside SCENARIO, for ~1 keV ENAs

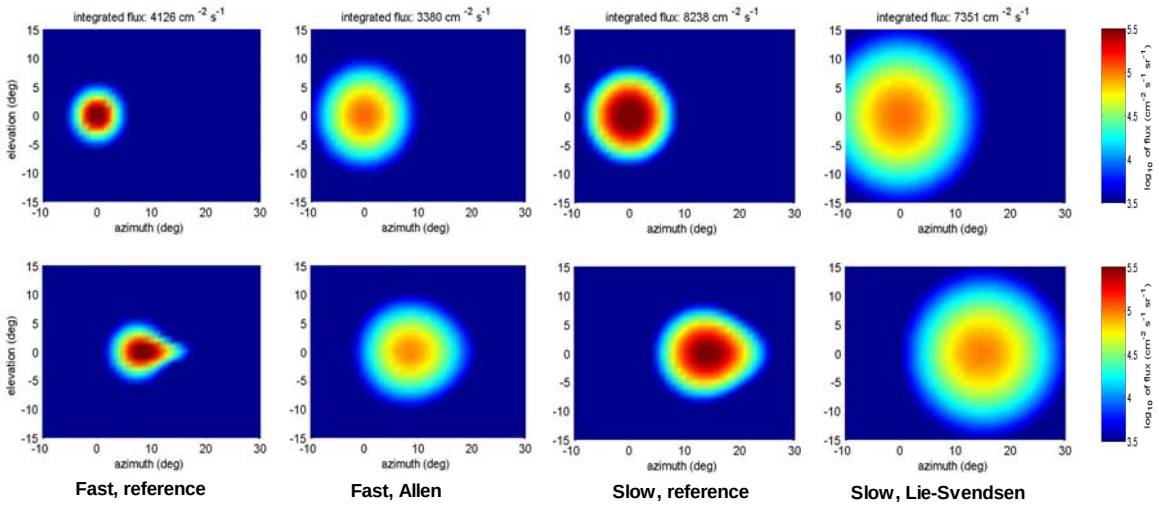

Figure 3.2. Pseudo-color map of differential flux as a function of angle from Sun's direction (in degrees) for different models. The azimuth angle is along the ecliptic plane, and the elevation angle is across the ecliptic plane. Flux is integrated over all energies (upper panels). Bottom panels are similar to upper ones, but the flux is calculated in the Solar Orbiter reference frame during the corotation phase (i.e. with the aberration effect included). The aberration effect is calculated by considering the actual energy distribution of the simulated signal.

Figure 3.1); 2) by using the shuttering system as a collimator, so that, by slowly changing the relative alignment of the two grid systems, make an angular scan through the FOV (12°×5°). In the latter case, the angular resolution is very good (1°×5°), since the information about the ENA direction is obtained before it impacts onto the ionizing surface, which introduces an angular scattering.

The energy (or velocity) resolution can be obtained in several ways. In fact, the ESA and the shuttering system have different operative modes (see Section 2 and 7), and the combination of these modes allows to:

- obtain the energy using the ESA as a fixed-biased dispersion plate, which focuses the output beam on the MCP target without the need of stepping energy
- obtain the energy using the ESA as a stepping-voltage, low-pass energy filter
- obtain the energy (the velocity) with a ToF analysis with triple or double coincidence.

Taking into account the previous considerations, and the fact that the ionizing surface introduces an energy straggling on the energy to be detected (10-15%, see Wieser and Wurz, 2002), the energy resolution dE/E can be estimated to be of the order of 25%.

3.3 Simulation of expected signal

Due to the spacecraft velocity, the detected solar wind properties will differ from those in the rest frame. In particular, at perihelion, the spacecraft has a tangential velocity of ~80 km/s. Since this value is comparable to the velocity of the neutral solar wind (~ 400 ÷ 700 km/s), this effect has to be taken into account. In fact, a detector placed on board SolO would "see" the protons and the neutrals as coming from a different direction

(aberration effect). A rough estimate gives a value between 5° and 10° (or more) for this effect depending on the SW velocity. This effect is illustrated in Figure 3.2 where the angular distribution is shifted and broadened in the azimuthal direction. The aberration effect is calculated by considering the actual energy distribution of the simulated signal.

Figure 3.3 shows the angular differential flux according to the slow SW simulation (total flux is about 8000 cm^{-2} s^{-1}); flux is integrated over all energies. The bottom-left panel is the corresponding instrument simulation. Figure 3.4 (top) shows the energy differential flux (same conditions), and the related instrumental simulation (bottom). Flux is integrated over all angles. To obtain these counts, we need to integrate for 1 min for every angular sector (or energy channel).

References

Wieser, M., and P. Wurz, NIMB 192, 370-380 (2002).

4 SUMMARY OF INSTRUMENT INTERFACES

4.1 SCENARIO Mass Budget

ITEM	Q.ty	MASS [g]	Contingency 20% [g]	Mass incl. Cont. 20% [g]
SENSOR MECHANICHS				
Lens group 1	1.0	30.0	6.0	36.0
Lens group 2	1.0	30.0	6.0	36.0
Plates Bearing	4.0	3.5	0.7	4.2
Plates Guides	4.0	6.8	1.4	8.2
Plates	2.0	55.0	11.0	66.0
Ultrasonic Oscillator	1.0	40.0	8.0	48.0
Lens group 3	1.0	30.0	6.0	36.0
Conversion Surface	1.0	2.8	0.6	3.4
ESA Grid + Bearing	1.0	25.0	5.0	30.0
MCP 1 Stop detector + Anode	1.0	60.0	12.0	72.0
NSWD BOX				
Base	1.0	132.0	26.4	158.4
Box Top Cover	1.0	42.0	8.4	50.4
Later wall 1	1.0	65.0	13.0	78.0
Lateral wall 2	1.0	65.0	13.0	78.0
Connector Box wall	1.0	48.0	9.6	57.6
Aperture wall	1.0	39.0	7.8	46.8
Locking Screws				
M3x6	24.0	22.8	4.6	27.4
Bearings				
High Voltage cards bearing	24.0	31.2	6.2	37.4
Sequencer/Communication Card	4.0	5.2	1.0	6.2
Encoder/decoder & Control	4.0	5.2	1.0	6.2
Prox Electronics bearing	4.0	5.2	1.0	6.2
Ultrasonic Oscillator bearing	4.0	3.0	0.6	3.6
ELECTRONICS				
HIGH VOLT Cards (30x75x15mm^3)	5.0	175.0	35.0	210.0
Piezo Driver (50x150x10mm^3)	1.0	75.0	15.0	90.0
Encoder/decoder & Control (50x150x10mm^3)	1.0	75.0	15.0	90.0
DC-DC Power Supply & Sequencer (160x100x15mm^3)	1.0	150.0	30.0	180.0
Proximity electronics (150x15x5mm^3)	1.0	25.0	5.0	30.0
CONNECTORS				
15 pin FEMALE	2.0	15.0	3.0	18.0
9 pin mini FEMALE	3.0	10.5	2.1	12.6
TOTALS				
TOTAL OPTICS	N/A	283.1	56.6	339.7

TOTAL BOX	**N/A**	**463.6**	**92.7**	**556.3**
TOTAL ELECTRONICS	**N/A**	**500.0**	**100.0**	**600.0**
TOTAL NSWD BOX		**1272.2**	**254.4**	**1526.6**
BAFFLE*				
Ext Collimator – body	**1.0**	**12.5**	**2.5**	**15.0**
Ext Collimator – plating	**1.0**	**14.5**	**2.9**	**17.4**
TOTAL SCENARIO		**1299.2**	**259.8**	**1559.0**
***Required if S/C body is not providing sun in the instrument FOV**				

4.2 SCENARIO Power Budget

ITEM	BLOCK ID	TYPE	Q.Ty	Power [mW]	+12V PWR %	-12V PWR %	+5V PWR %	-5V PWR %	+12V Curr (mA)	-12V Curr (mA)	+5V Curr (mA)	-5V Curr (mA)
1	HV Supply provision	HV COLLIMATOR BIAS	2	700.0	50.00%	50.00%	0.00%	0.00%	29.2	29.2	0.0	0.0
2	HV Supply provision	HV MCP BIAS	1	350.0	50.00%	50.00%	0.00%	0.00%	14.6	14.6	0.0	0.0
3	HV Supply provision	LENS 1, 3	1	350.0	50.00%	50.00%	0.00%	0.00%	14.6	14.6	0.0	0.0
4	HV Supply provision	ESA HV	1	350.0	50.00%	50.00%	0.00%	0.00%	14.6	14.6	0.0	0.0
5	HV Supply provision	LENS 2	1	350.0	50.00%	50.00%	0.00%	0.00%	14.6	14.6	0.0	0.0
6	Motor Driver	106RH Motor Driver (disabled)*	1	50.0	50.00%	50.00%	0.00%	0.00%	2.1	2.1	0.0	0.0
7	Motor Driver	AD630	1	25.0	0.00%	0.00%	50.00%	50.00%	0.0	0.0	2.5	2.5
8	Motor Driver	AD9835	1	200.0	0.00%	0.00%	50.00%	50.00%	0.0	0.0	20.0	20.0
9	Motor Driver	AD526	1	140.0	0.00%	0.00%	50.00%	50.00%	0.0	0.0	14.0	14.0
10	Motor Driver	AD522	1	100.0	0.00%	0.00%	50.00%	50.00%	0.0	0.0	10.0	10.0
11	Encoder/Decoder	OP467	1	50.0	0.00%	0.00%	50.00%	50.00%	0.0	0.0	5.0	5.0
12	Encoder/Decoder	AD790	1	60.0	50.00%	50.00%	0.00%	0.00%	2.5	2.5	0.0	0.0
13	Encoder/Decoder	HS-22620	1	50.0	0.00%	0.00%	50.00%	50.00%	0.0	0.0	5.0	5.0
14	Encoder/Decoder	HI-201HS-2	1	50.0	0.00%	0.00%	50.00%	50.00%	0.0	0.0	5.0	5.0
15	Encoder/Decoder	AD637	1	30.0	0.00%	0.00%	50.00%	50.00%	0.0	0.0	3.0	3.0
16	Proximity	2N2907A	1	10.0	0	0	100.00%	0.00%	0.0	0.0	2.0	0.0
17	Proximity	2N2222A	1	5.0	0	0	100.00%	0.00%	0.0	0.0	1.0	0.0
18	Proximity	AD8031a/AD	1	10.0	0	0	50.00%	50.00%	0.0	0.0	1.0	1.0
19	Proximity	AD8021	1	35.0	0	0	50.00%	50.00%	0.0	0.0	3.5	3.5
20	Proximity	ADR421	1	5.0	0	0	100.00%	0.00%	0.0	0.0	1.0	0.0
21	Proximity	AD7671	1	125.0	0	0	100.00%	0.00%	0.0	0.0	25.0	0.0
22	Proximity	ADuM1400BRW	1	15.0	0	0	100.00%	0.00%	0.0	0.0	3.0	0.0
23	Proximity	AD580JH	1	5.0	0	0	100.00%	0.00%	0.0	0.0	1.0	0.0
24	Proximity	OP27	5	75.0	0	0	50.00%	50.00%	0.0	0.0	7.5	7.5
25	Proximity	OPA627AU	4	120.0	0	0	50.00%	50.00%	0.0	0.0	12.0	12.0
26	Proximity	ADuM1401BRW	2	30.0	0	0	75.00%	25.00%	0.0	0.0	4.5	1.5
27	Proximity	OP176GS	1	10.0	0	0	50.00%	50.00%	0.0	0.0	1.0	1.0
28	Proximity	AD8561	1	30.0	0	0	100.00%	0.00%	0.0	0.0	6.0	0.0
29	Proximity	OP275GS	1	30.0	0	0	50.00%	50.00%	0.0	0.0	3.0	3.0
30	Proximity	LM324/SO	3	30.0	0	0	50.00%	50.00%	0.0	0.0	3.0	3.0
31	Proximity	AD8842AR	1	70.0	0	0	50.00%	50.00%	0.0	0.0	7.0	7.0
32	Main	AD7490BRU	1	10.0	0	0	100.00%	0.00%	0.0	0.0	2.0	0.0
33	Main	RTAX1000S	1	600.0	0	0	100.00%	0.00%	0.0	0.0	120.0	0.0
34	Main	ADP3334AR	1	50.0	0	0	100.00%	0.00%	0.0	0.0	10.0	0.0
35	Main	AT28C010	2	150.0	0	0	100.00%	0.00%	0.0	0.0	30.0	0.0
36	Main	TLV2217-33	1	100.0	0	0	100.00%	0.00%	0.0	0.0	20.0	0.0
37	Main	LM117	1	75.0	0	0	100.00%	0.00%	0.0	0.0	15.0	0.0
38	Main	ASIC AFE	1	130.0	0	0	50.00%	50.00%	0.0	0.0	13.0	13.0
39	Main	LM317H/TO	1	75.0	0	0	100.00%	0.00%	0.0	0.0	15.0	0.0
40	Main	AT60142E	2	220.0	0	0	100.00%	0.00%	0.0	0.0	44.0	0.0
41	Main	54ACT16240/FP	1	20.0	0	0	100.00%	0.00%	0.0	0.0	4.0	0.0

42	Main	54ACT16245/FP	2	20.0	0	0	100.00%	0.00%	0.0	0.0	4.0	0.0
43	Main	OSC-50MHz	1	45.0	0	0	100.00%	0.00%	0.0	0.0	9.0	0.0
	MODE REST/HIGH TRASM	TOTAL POWER ON SEC PWR BUS		4955.0					92.1	92.1	432.0	117.0
	MODE REST/HIGH TRASM	TOTAL POWER ON PRI PWR BUS (75%)		6606.7								
6/b	Motor Driver	106RH Motor Driver (Enabled)	1	500.0	50.00%	50.00%	0.00%	0.00%	20.8	20.8	0.0	0.0
	MODE LOW/ANGULAR SCAN	TOTAL POWER ON SEC PWR BUS		5405.0					110.8	110.8	432.0	117.0
	MODE LOW/ANGULAR SCAN	TOTAL POWER ON PRI PWR BUS (75%)		7206.7								
6/c	Motor Driver	106RH Motor Driver (Enabled)	1	1200.0	50.00%	50.00%	0.00%	0.00%	50.0	50.0	0.0	0.0
	MODE FAST TOF RES	TOTAL POWER ON SEC PWR BUS		6105.0								
	MODE FAST TOF RES	TOTAL POWER ON PRI PWR BUS (75%)		8140.0					140.0	140.0	432.0	117.0

4.3 SCENARIO Telemetry Budget

Mode	Countrate (s^{-1})	Bin matrix	Time res. (s)	Telemetry (bit/s)	Remarks
Raw	100	N/A	1	2500	see Section 7.2
Raw[(1)]	1000	N/A	1	25000	see Section 7.2
Binning, Nominal	**<1000**	**16 Energies × 12 Angles**	**60**	**50**	**16×12×16/60**
Binning[(2)]	<1000	128 Energies × 12 Angles	60	205	128×12×8/60
Binning[(2)]	<1000	128 Energies	60	35	128×8/60
Binning[(2)]	<1000	12 Angles	60	4	12×8/60
Calibration	N/A	N/A	1	100	see Section 7.3

(1) for extreme events
(2) each channel can contain up to 2^{16}, log compressed, counts. The maximum countrate is $2^{16}/60$ s = 1000 s^{-1}

5 TEST AND CALIBRATION PLAN

5.1 Modelling

From a thermal point of view, SCENARIO does not foresee any critical device. Hence, thermal models will take care of dissipation of electronics/ultra-sonic oscillator thermal inputs. Such models will demonstrate that SCENARIO complies with system requirements, and will be delivered according to EID-A indications.
Signal processing model will be developed according to EID-A requirements.

5.2 Ground Testing and Calibration

The critical elements tests and qualification will be performed at IFSI, including the MCP efficiency. The grids will be qualified in the frame of BepiColombo SERENA project. The manufacturing process of the shuttering system will be performed at CNR-IFN. The IFSI calibration facility will be used for tests of energetic neutral atoms for development, laboratory and engineering models. The ionizing surface calibration activity will be done at the University of Bern. For other models we will use the clean room at the CNR/INAF "Tor Vergata" Area (ARTOV). At the University of Bern the check of the whole experiment SCENARIO will be eventually done.

5.3 In-flight Calibration

No specific calibrations procedures are foreseen for cruise phase. During in-orbit phases no periodic calibration activities are foreseen. Occasional calibration activities will be performed by specific procedures through telecomand (TLC).

6. SYSTEM LEVEL ASSEMBLY, INTEGRATION AND VERIFICATION

6.1 Requirements

The SCENARIO qualification flow will comply with the project provided pre-launch verification program requirement (see EID-A) and the spacecraft system level AIV flow. The SCENARIO PI shall establish and conduct a full instrument level AIV program and provide support to the system level AIV program.

Assembly Integration and Verification activities will be performed at IFSI. SCENARIO will be integrated in the 100000-class clean room (200 m^2) available at ARTOV.

6.2 Deliverable Models

STM, EM, FM will be developed and delivered according to the program plan. A QM will be developed for qualification testing. The QM will be developed at flight level quality becoming a FM spare.

6.3 System Level Testing

The SCENARIO PI shall support the system level integration and test activities related to and involving the instrument. This includes the System Validation Tests, involving the spacecraft and the ground segment. All the flight procedures foreseen for the single segments for the orbit and mission will be locally simulated and verified by the SCENARIO EGSE, described the EID-B section.

7 FLIGHT OPERATIONS CONCEPT

7.1 Normal operations

The nominal operational mode of the SCENARIO unit is based on automatic procedures, which do not require any specific assistance. Mode of operation changes may be necessary at times during in-orbit phases. The SCENARIO team will support the MOC and SOC as required. Specifically:

- The team will take care of supporting during cruise science operations
- The SCENARIO experiment will need support of a technical expert of the software tools for the interfaces management during payload commissioning and critical operations.
- The SCENARIO experiment will need support of a technical expert of TLC during the science operations phase.

The SCENARIO sensor shuttering system may be set into at least three different configurations:

- at rest position (high transparency mode, low angular resolution);
- low-frequency (used as a collimator, with azimuth angular scanning within 12°, high angular resolution);
- high-frequency (used as START signal).

The electrostatic mirror (located just after the ionizing surface) can operate according to three different approaches:

- fixed (highest voltage, for maximum efficiency);
- stepping (for resolving energy steps of energy resolution of about 25%);
- on/off (electronic gate at high frequency), to provide triple-coincidence ToF measurements.

7.2 Telemetry modes

For each of the operative modes described in Section 7.1, SCENARIO can use two basic telemetry modes: raw mode and binning mode (see table in Section 4.3). In raw mode, each particle targeting is processed separately and results in a telemetry event of 4 bits (angular scanning) + 12 bits (ToF1) + 2 bits (Coincidence) + 7 bits (128 Chs., MCP anode information). Considering an average countrate up to100 s^{-1}, the telemetry bitrate is up to 2500 b/s; considering an extreme event, with a countrate of 1000 s^{-1}, the highest telemetry bitrate is 25000 b/s.

In triple coincidence mode, additional 12 bits ToF information is foreseen, but the angular scanning is disabled (angle is resolved by means of the MCP anode information). Hence, the telemetry bitrate is (12+12+2+7)×100=3300 b/s.

In binning mode, a matrix of up to 128 ToF or energy channels, and up to 12 angular channel is transmitted, i.e. a maximum of 128×12=1536 channels. Assuming 8 bits for each channel (log compression), and for a nominal resolution time of 60 s, this results in a maximum bitrate of 205 b/s. Different configuration of the bin matrix can be used, resulting in different bitrates (see table in Section 4.3). The nominal mode foresees 16 energy channels ×12 angular sectors ×16 bit/channel. With a time resolution of 60 s, the bitrate is 50 b/s.

7.3 Other modes

7.3.1 Calibration mode

Besides the basic modes described in Section 7.1, both the ESA and the shutter system can be set in "calibration" mode: for example, closing the shutter, and switching off the ESA voltage, to study the background/noise signal. The telemetry will be, at maximum, the one of the raw mode.

8 DATA REDUCTION AND SCIENTIFIC ANALYSIS PLANS

8.1 Data Processing and Standard Data Products

A preliminary data reduction and scientific analysis plan foresee:

- Pre-launch: developing codes for proper extraction of the SCENARIO data from the spacecraft telemetry and for data display;
- Support to the Science Operation Centre (SOC): SCENARIO team experts will attend SOC activities and provide needed information;
- Cruise phase: the SCENARIO team will support all specific activities foreseen for the instrument units, providing a detailed schedule;

- Operations phase: nominal instrument operations will be constantly monitored by the SCENARIO team; any critical action will be properly requested accordingly to the foreseen general SOC procedures; the SCENARIO team will provide a detailed schedule of operational mode changes;

- Science analysis: a preliminary analysis of the scientific data will be performed in quasi-real time in order to check the reliability of the scientific outcome and for possible prompt actions on the operation schedule; specific data analysis and scientific interpretations will be performed by the SCENARIO team and, after the proprietary period by the rest of the international scientific community;

- Archival phase: it will be performed in parallel with the preliminary data analysis.

8.2 Specific Software Products

C-, Fortran-, Matlab- and IDL-based codes will be developed for proper presentation, web distribution and analysis of SCENARIO science and housekeeping data.

8.3 Software Product and Procedure Standards

Matlab, IDL, SIMION will be used for data analysis and instrument simulations.

8.4 Compliance with Science Data Policy defined in SolO Science Management Plan

Science operations will be conducted in close coordination with SOC. The PI will receive the raw data, the instrument and spacecraft housekeeping from MOC and will distribute them to the Team Leaders and Co-Is. Reduction of science data is under the responsibility of the SCENARIO team. The SCENARIO science management plan will comply the science operation plans, the data handling and archiving concepts as defined by the SOC. After proprietary period of 6 months, the data will be delivered to the SolO scientific archive for public domain within the other SolO scientists and the whole scientific community.
Specifically, the SCENARIO PI will take responsibilities as in the following:

- support the definition of the science operations;
- Provision of inputs for the definition and implementation of the science operations planning, and data handling and archiving concepts;
- Support the preparation of the instrument operation timelines;
- Provide expert support at the MOC during payload commissioning and critical operations
- Support of the definition and implementation of the SolO scientific data archive, as part of the pre-launch tasks;
- Provision of support required by the SOC and other PI's for science planning purposes;
- Monitoring and optimisation of instrument performance;
- Deliver raw, calibrated, and high level data, including relevant calibration products, to the SolO scientific archive, at the end of the proprietary period;
- Provision to ESA with unlimited access to all processed and analysed data for public relation purposes;

- Provision of summaries of the main scientific results at regular intervals.

9 PROGRAMMATIC

Compliance with Programme Requirements of EID-A: no critical issues are foreseen in terms of Programme Requirements.

- Schedule: The instrument reviews will take place according to the following reviews: IPDR, ICDR, IQR, IFAR. The SCENARIO Thermal Mathematical Model and Structural Mathematical Model issues will be updated according to the requests of the planning.

Management: In order to comply with EID-A requirements (described in Section 6), the SCENARIO team structure and organization has been simplified and optimized to minimize any programmatic risks. Details on the management are presented in the management plan document. Generally, the management structure foresees a PI (Dr. Stefano Orsini) responsible of the whole instrument, and two project scientists: Dr. Martin Hilchenbach and Dr. Ke Chiang Hsieh. SCENARIO is supervised by a project manager (Dr. Andrea M. Di Lellis) who will lead a team composed by the specific subunits technical managers. The SCENARIO PI will ensure the development, construction, testing and delivery of the instrument. This will be performed in accordance with the standards, technical and programmatic requirements defined in the Experiment Interface Document (EID). SCENARIO science studies will be carried by a Science Team coordinated by Dr. Shadia Rifai Habbal.

Deliveries: SCENARIO deliveries will be in line with the overall project constraint

- STM: 17/06/2011
- EM: 22/06/2012
- FM: 28/06/2013

The FS will be available about 6 months after the delivery of the FM.

10 Annex 1:

10.1 Qualifications and Experience of PI Team and Key Staff

The SCENARIO team has gained relevant experience through a very long and successful heritage of space projects, actively participating to most of the major present and past ESA and NASA programs devoted to interplanetary space particle investigations as well as to planetary exploration. Among these programs, it is worth mentioning still operating or ongoing missions, like BepiColombo, CLUSTER, MARS EXPRESS, ROSETTA, DOUBLESTAR, VENUS EXPRESS, and NASA IMAGE, CASSINI and MESSENGER.

The SCENARIO Science Team incorporates most of the world experts in ENA imaging, including PIs and Co-Is of ENA instrumentation on board space missions devoted to both planetary exploration and space weather. Moreover, qualified experts of the heliosphere environment are present in the team as well. The Project management together with the associated Technical Team ensures high quality technical production, given the past involvement in top-level technology applied to space instrumentation.

Istituto di Fisica dello Spazio Interplanetario (IFSI, Rome, Italy), the PI Institute, is presently part of the "Istituto Nazionale di Astrofisica" (INAF). IFSI has been involved in space research since 1968, and throughout these 39 years of qualified work it has reached top international levels in both space science and space technology. Similar arguments are valid for the four major partner institutes (UniBe, CESR, FMI, and SRC), as well as for the rest of the SCENARIO team.

More details on team expertise may be found in the Management Plan Document, where CVs of all Team Leaders, Co-Is and team key persons are also given.